LPV Aeroservoelastic Control using the LPVTools Toolbox

Arnar Hjartarson,[*] Peter J. Seiler,[†] and Gary J. Balas[‡]

LPVTools is a MATLAB toolbox that is being developed to perform gain-scheduled Linear Parameter-Varying (LPV) control of aeroservoelastic systems. This paper outlines the LPV modeling, analysis and controller synthesis features of this toolbox. The features of the toolbox are illustrated by an application example, where a grid-based LPV model is developed for the X-56A aircraft using LPVTools. The X-56A Multi Utility Technology Testbed, funded by the US Air Force and designed by Lockheed Martin's Skunk Works, is a modular uninhabited aircraft designed to test active flutter suppression and gust load alleviation algorithms. The X-56A example shown in this paper demonstrates how LPVTools can be used to develop LPV gain scheduled controllers for a aeroservoelastic systems.

I. Introduction

Gain scheduling via interpolation of point designs is the predominant method used in industry to develop a full-envelope flight control law. LPV analysis can play an important role in certifying the performance of these control laws. Moreover, LPV analysis tools can uncover potential stability and performance degradations caused by rapid variations in the operating condition. This is especially important for systems with significant aeroelastic effects because flexible modes may be excited during aircraft maneuvers. LPVTools is a software suite, implemented in MATLAB , that simplifies modeling and control design in the LPV framework. Furthermore, LPVTools simplifies the analysis of gain-scheduled LPV control laws in both the LTI- and the LPV-framework.

This paper provides an overview of the LPVTools software suite. A brief outline of the underlying LPV modeling framework is presented, along with a survey of the tools provided by the software suite to perform synthesis and analysis of LPV systems. The X-56A Multi Utility Technology Testbed is used to demonstrate the capabilities of the software tools.

The remainder of the paper is divided up into five sections. First, an overview of the LPVTools software suite is given in Section II. Next, the X-56A rigid body and aeroelastic dynamics are described in Section III. A reduced order model of the X-56A is developed in Section IV, and grid-based LPV control laws are designed and analyzed in Section V. Finally, conclusions are given in Section VI.

II. The LPVTools Software Suite

MUSYN Inc. is developing software tools to aid in modeling, analysis, controller synthesis, and simulation of Linear, Parameter-Varying (LPV) systems. One key component of this work is the development of parameter-varying data structures for modeling of LPV systems within the MATLAB /SIMULINK software environment.

Linear Parameter Varying models are time-varying, state-space models of the form:

$$\begin{bmatrix} \dot{x}(t) \\ y(t) \end{bmatrix} = \begin{bmatrix} A(\rho(t)) & B(\rho(t)) \\ C(\rho(t)) & D(\rho(t)) \end{bmatrix} \begin{bmatrix} x(t) \\ u(t) \end{bmatrix} \tag{1}$$

where $A(\rho(t))$ is the state matrix, $B(\rho(t))$ is the input matrix, $C(\rho(t))$ is the output state matrix, $D(\rho(t))$ is the input transformation matrix, $\rho \in \mathbb{R}^{n_\rho}$ is a vector of measurable parameters, $y \in \mathbb{R}^{n_y}$ is the measurement, and $u \in \mathbb{R}^{n_u}$ is the control input.

---

[*]MUSYN Inc., arnar.hjartarson@musyn.com
[†]MUSYN Inc., peter.j.seiler@gmail.com
[‡]MUSYN Inc., balas@musyn.com

American Institute of Aeronautics and Astronautics

Several methods have arisen for representing the parameter dependence in LPV models (Equation 1). These include linear fractional transformations,[1–6] linearizations on a gridded domain,[7–10] and polytopic (affine) dependence of the state matrices on the parameters.[11–14] Each of these different representations has benefits and drawbacks in terms of the modeling effort and model structure that can be exploited in developing computational algorithms. As a starting point, the initial implementation of the LPV toolbox focuses on models defined on gridded domains and models represented by linear fractional transformations.

A. Grid-based LPV Model

An LPV model that is defined on a gridded domain is pictorially represented in Figure 1. Grid-based LPV models are motivated by aircraft aeroelastic control problems for which models are typically constructed as linearizations of the aircraft's nonlinear dynamics around various flight operating points.

A key component of the grid-based LPV software tools is a core LPV data structure object, referred to as a `pss` (denoting parameter-varying state space model). In the grid-based LPV framework, the LPV systems in Equation 1 are conceptually represented by a state-space system S that depends on a parameter vector ρ in some domain of $\mathbb{R}^{n_\rho}$. For general LPV systems this conceptual representation requires storing the state space system at an infinite number of points in the domain of ρ. The data structure object `pss` approximates this conceptual representation by storing the LPV system as a state space array defined on a finite, gridded domain. As a simple example, consider an LPV system $S(\rho)$ that depends on a single parameter ρ in the domain $\rho \in [a, b]$. The infrastructure requires the user to specify the domain with a finite grid, e.g. N points in the interval $[a, b]$. The toolbox contains an `rgrid` data object to facilitate the creation and manipulation of the multivariable parameter domains. The user must also specify the values of the state space system S at each point ρ in this gridded domain. The `pss` object stores the state-space array data using the standard MATLAB Control System Toolbox `ss` object. Thus the `pss` can be viewed as the parameter-varying extension of the standard `ss` object. To summarize, the LPV system $S(\rho)$ is represented by a `pss` data object which stores the gridded domain and the array that defines the state-space data at each point in the domain.
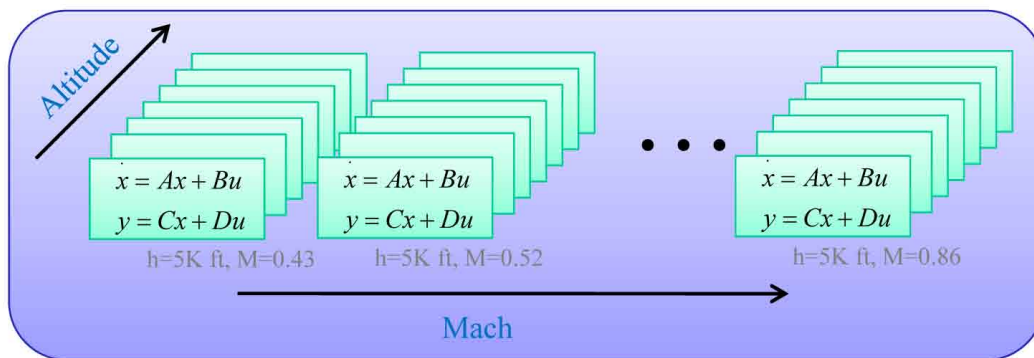
Figure 1. LPV models defined on a rectangular grid

The notions of parameter-varying matrices and parameter-varying frequency responses arise naturally to complement the `pss` objects. LPV systems are time-varying and hence frequency responses can not be used to represent the system behavior as parameters vary. However frequency responses are useful to gain intuition about the system performance at fixed locations in the operating domain. LPVTOOLS represents parameter varying matrices and frequency responses by `pmat` and `pfrd` data objects, respectively. These two data objects are both stored as a data array defined on a gridded domain. Table 1 shows the relation between the core grid-based LPVTOOLS data objects (`pmat`, `pss`, `pfrd`) and existing MATLAB objects. The first row of the Table ("Nominal") shows the basic MATLAB objects: matrices are `double` objects, state-space systems are `ss` objects, and frequency responses are `frd` objects. `double` objects are in the standard MATLAB release while the `ss` and `frd` objects are part of the Control System Toolbox. The second row of Table 1 ("Parameter Varying") shows the core LPV objects. The main point is that the (`pmat`, `pss`, `pfrd`) objects should be viewed as parameter-varying extensions of the standard MATLAB and Control Toolbox objects (`double`, `ss`, `frd`).

American Institute of Aeronautics and Astronautics

Object Type	Block	Matrix	System	Frequency Response
Nominal	$y \leftarrow \boxed{M} \leftarrow u$	double	ss	frd
Parameter Varying	$y \leftarrow \boxed{M(\rho)} \leftarrow u$	pmat	pss	pfrd
Uncertain	$\boxed{\Delta}$ $y \leftarrow \boxed{M} \leftarrow u$	umat	uss	ufrd
Uncertain Parameter Varying	$\boxed{\Delta}$ $y \leftarrow \boxed{M(\rho)} \leftarrow u$	upmat	upss	upfrd
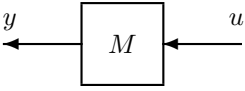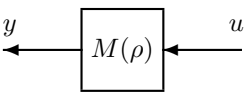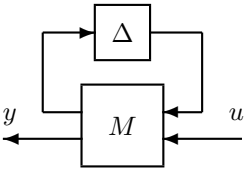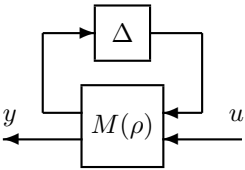
Table 1. Relation between MATLAB objects

The third row of the table ("Uncertain") shows the equivalent objects used to represent uncertainty: uncertain matrices, state space systems, and frequency responses are represented by umat, uss, and ufrd objects, respectively. These objects are part of the MATLAB Robust Control Toolbox. The Robust Control Toolbox models the uncertainty as a perturbation Δ wrapped in feedback around a nominal part M, i.e. uncertainty is represented using a linear fractional transformation. Real parametric, complex parametric, and unmodeled dynamic uncertainties can be modeled. The last row of Table 1 ("Uncertain Parameter Varying") shows the corresponding parameter-varying objects with uncertainty: uncertain parameter-varying matrices, state space systems, and frequency responses are represented by upmat, upss, and upfrd objects, respectively. These objects enable the integration of uncertainty into grid-based LPV models.

It is important to note that all LPV objects are being developed within MATLAB's object-oriented programming framework. A benefit of object-oriented programming is that key operations can be overloaded to provide seamless, consistent functionality across a variety of objects. For example, if A and B are double objects then the syntax A*B simply multiplies the matrices. If A and B are pmat objects then the syntax A*B multiplies the parameter-varying matrices at each point in the parameter domain. The manipulation of parameter-varying objects is facilitated by this extension of the * operation to a meaningful, intuitive operation for pmat objects. In addition, standard MATLAB syntaxes, e.g. M(i,j) to index into the (i, j) element of an array, have been overloaded and extended for parameter-varying objects. Object-oriented programming enables this overloading of key functions and this enables meaningful, intuitive extensions for parameter-varying objects.

One objective for the LPV toolbox, LPVTOOLS, is to expand the functionality and tools for LTI systems, as developed in the MATLAB Control and Robust Control Toolboxes, to linear parameter-varying systems. Table 1 shows the relation between the grid-based LPV data objects that are implemented in LPVTOOLS and their current Control/Robust Control Toolbox counterparts. It is also worth mentioning that MATLAB SIMULINK contains blocks to model and simulate double, ss, uss objects. LPVTOOLS also includes SIMULINK blocks for simulation and real-time implementation. To summarize, the core infrastructure for grid-based LPV systems currently includes objects to model the parameter domain (rgrid), nominal and uncertain parameter-varying matrices (pmat, upmat), nominal and uncertain LPV state-space systems (pss, upss), and nominal and uncertain parameter-varying frequency response models (pfrd, upfrd).

American Institute of Aeronautics and Astronautics

B. LFT-based LPV Model

An LPV model in Linear Fractional Transformation (LFT) form is an interconnection of a block that represents the plant's nominal dynamics (linear), and a block that contains the time-varying parameters, which the system depends on. The LFT framework can be used to model LPV models with rational parameter dependence.[15, 16] In the LFT-based framework the LPV system in Equation 1 is expressed as the interconnection of the blocks M and Δ_ρ, shown in Figure 2, where M is a constant matrix

$$M = \begin{bmatrix} D_{zw} & D_{zu} & C_z \\ D_{yw} & D_{yu} & C_y \\ B_w & B_u & A \end{bmatrix} \tag{2}$$

such that

$$\begin{bmatrix} z(t) \\ y(t) \\ \dot{x}(t) \end{bmatrix} = \begin{bmatrix} D_{zw} & D_{zu} & C_z \\ D_{yw} & D_{yu} & C_y \\ B_w & B_u & A \end{bmatrix} \begin{bmatrix} w(t) \\ u(t) \\ x(t) \end{bmatrix} \tag{3}$$

and Δ_ρ is a diagonal matrix

$$\Delta_\rho = \begin{bmatrix} \rho_1(t)I_{r_1} & 0 & \cdots & 0 \\ 0 & \rho_2(t)I_{r_2} & \cdots & 0 \\ \vdots & \vdots & \ddots & \vdots \\ 0 & 0 & \cdots & \rho_{n_\rho}(t)I_{r_{n_\rho}} \end{bmatrix} \tag{4}$$

that depends on n_ρ time-varying parameters, such that

$$w(t) = \begin{bmatrix} \rho_1(t)I_{r_1} & 0 & \cdots & 0 \\ 0 & \rho_2(t)I_{r_2} & \cdots & 0 \\ \vdots & \vdots & \ddots & \vdots \\ 0 & 0 & \cdots & \rho_{n_\rho}(t)I_{r_{n_\rho}} \end{bmatrix} z(t) \tag{5}$$

where I_{r_1} indicates a r_1-by-r_1 identity matrix.
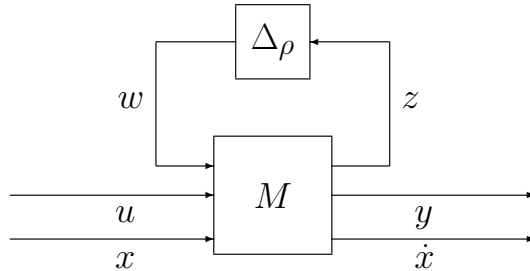
Figure 2. An LPV system in LFT form.

A key component of the LFT-based LPV software tools is a core LPV data structure object, referred to as a `tvreal` (denoting a time-varying parameter). The `tvreal` object is used to create a time-varying, real valued scalar object. The `tvreal` has a range, denoting the maximum and minimum value that the time-varying scalar can assume, and a rate-bound denoting the maximum and minimum rate of change of

American Institute of Aeronautics and Astronautics

the time-varying scalar. The `tvreal` is used to model the individual time-varying parameters from which parameter dependent LFT matrices and LFT systems are defined. The `tvreal` serves as a building block for LFT based LPV matrices and systems, similar to how a `ureal` serves as a building block for `umat` and `uss` objects in the Robust Control Toolbox.

LPVTOOLS represents LFT-based parameter varying matrices and state-space systems by `plftmat` and `plftss` data objects, respectively. The `plftmat`, and `plftss` objects are constructed using `tvreal` elements, using a syntax that is a direct parallel to the syntax that is used to define `umat` and `uss` objects in the Robust Control Toolbox. Both `plftmat` and `plftss` objects are stored as uncertain objects (i.e. `umat` and `uss`, respectively) with the constituent `tvreal` objects providing the additional information necessary to handle the uncertainty like a time-varying parameter. Uncertainty can be integrated into the `plftmat`, and `plftss` objects, allowing these data objects to model system with and without uncertainty. The `plftmat` and `plftss` objects should be viewed as LFT-based parameter-varying extensions of the standard MATLAB and Control Toolbox objects `double` and `ss`, respectively.

C.   Transition Between Grid-based and LFT-based LPV Models

Transition between grid-based (i.e. `pmat`, `pss`) and LFT-based (i.e. `plftmat`, or `plftss`) LPV models is possible using the `grid2lft` and `lft2grid` functions in LPVTOOLS. The `lft2grid` function transforms LFT-based LPV models into grid-based LPV models by evaluating the the LFT-based model at a grid of parameter values. The user can specify this grid explicitly or allow the `lft2grid` function to derive a grid based on each parameter's range.

The `grid2lft` function transforms an grid-based LPV model into a LFT based LPV model. For a grid-based LPV data object, the object contains an array of data defined on a grid of parameter values. The `grid2lft` function is designed to approximate the parameter dependence of the underlying data, and express it as a rational function that can be rewritten in LFT form. The current implementation is restricted to polynomial parameter dependence.

As an example, the parameter varying matrix that is modeled by a `pmat` is stored as an array of matrices defined on a grid of parameter values. The function attempts to fit each individual matrix element of the parameter-varying matrix with a polynomial, that depends on the time-varying parameters. This polynomial describes how the value of the matrix element changes as a function of the parameters. The parameter dependence of the `pmat` object has been approximated once each element of the parameter varying matrix has been fitted with a polynomial. The polynomial in each element of the matrix can then be transformed into LFT form, and the whole matrix thus transformed into LFT-based LPV form. A similar procedure applies to `pss` objects, where the parameter dependent (A,B,C,D) matrices of the parameter dependent state-space system are transformed into LFT form in order to obtain an LFT-based LPV system.

Obtaining minimal realizations of the LFT system, i.e. a system that has the least number of repeated parameters in the Δ_ρ block of the LFT interconnection, is an open problem.[16–20] Repeated blocks increase the computational complexity of applying synthesis and analysis tools to the resulting LFT models. The polynomial fitting methodology employed in the `grid2lft` function often yields non-minimal models, with many repeated parameters in the parameter block of the LFT interconnection. Future work will refine the algorithms that are implemented in `grid2lft` to take advantage of recent results which focus on ways to reduce the number of repeated parameters in the resulting LFT models.[17–19]

D.   LPV Synthesis and Analysis Tools

LPVTOOLS includes overloaded versions of several analysis functions from the Robust Control Toolbox (e.g. `wcgain`, `robustperf`,`robuststab`). These functions are applicable to grid-based LPV systems only. They can be used to study the properties of the LPV system point-by-point in the parameter domain, i.e. the analysis is performed on the Linear Time Invariant (LTI) system that is obtained when the time-varying parameter is frozen at a specific value.

LPVTOOLS contains the function `lpvnorm` to compute an upper bound on the induced L_2 norm for an LPV system. `lpvnorm` is implemented both for grid-based and LFT-based LPV systems. For grid-based LPV systems the L_2 norm of the system is computed using conditions based on results by Wu, et al.,[9] while for LFT-based LPV systems the L_2 norm of the system is computed using conditions based on results by Apkarian, et al.[5,6]

American Institute of Aeronautics and Astronautics

LPVTools provides a function `lpvsyn` to synthesize output feedback controllers for LPV systems. The synthesis conditions that are used by `lpvsyn` are developed starting from the L_2 gain conditions used by `lpvnorm`. For grid-based models the synthesis conditions are based on the results by Wu, et al.[9] and Lee,[21] while the synthesis conditions for LFT-based models are provided by the results of Apkarian, et al.[5, 6]

E.   LPV Model Reduction Tools

Model reduction of LPV systems is possible using LPVTools . The function `pbalancmr` implements a Balanced Truncation of an LPV model (analogous to a balanced truncation of an LTI system[22]), while the function `pncfmr` implements a Contractive Coprime Factorization of an LPV model (analogous to a Normalized Coprime Factorization of an LTI or LTV system.[23]) Both methods are restricted to grid-based LPV models, and are based on results derived by Wood.[24, 25] The method of Contractive Coprime Factorization is applicable to both stable and unstable LPV systems, but the method of balanced truncation is restricted to stable LPV systems.

III.   X-56A Aircraft

The X-56A linear models were provided to MUSYN Inc by NASA Dryden researchers. These models are representative of straight and level flight condition at 7 different velocities. The X-56A model considered has 14 structural modes. Figure 3 shows the damping values and normalized natural frequencies, ω_n/ω_{ref}, for the modes as a function of normalized air speed, V/V_{ref}. The aircraft is stable at the first three flight condition, but the body freedom flutter mode becomes unstable at $V/V_{ref} = 0.83$, the first symmetric bending mode becomes unstable at $V/V_{ref} = 0.92$ and the first anti-symmetric mode goes unstable at $V/V_{ref} = 1$.
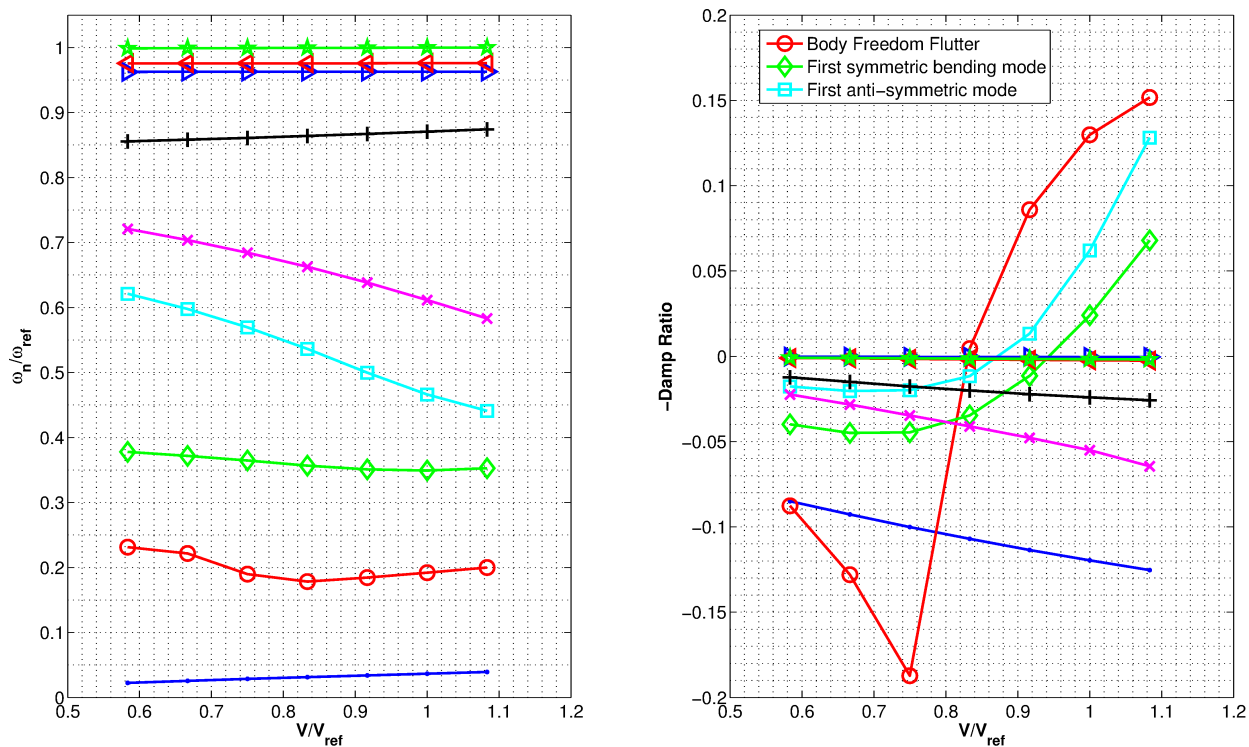
Figure 3. X-56A Natural Frequencies and Damping Across Flight Condition

The linear state space models, G, are of the form

$$\dot{x} = A_p x + B_p u \tag{6}$$
$$y = C_p x + D_p u \tag{7}$$

American Institute of Aeronautics and Astronautics

where the A_p, B_p, C_p, and D_p matrices can be described as

$$[A_p] = \begin{bmatrix} A_{rr} & A_{re} & B_{rr} \\ A_{er} & A_{ee} & B_{re} \\ 0 & 0 & A_{act} \end{bmatrix}, \quad [B_p] = \begin{bmatrix} 0 \\ 0 \\ B_{act} \end{bmatrix}, \quad [C_p] = [C_{ae} \quad D_{ae}], \quad [D_p] = 0$$

The state vector is defined as $x = \{x_{AS}, x_\zeta, x_{act}\}$, where x_{AS} corresponds to airframe rigid body states, x_ζ corresponds to the elastic and aerodynamics states, and x_{act} corresponds to the actuator states. The matrix subscripts correspond to actuator (act), rigid body (r), elastic (e), aeroelastic (ae), and plant (p). The airframe rigid body states are

$$x_{AS} = \{x, h, \theta, u, \alpha, q, y, \beta, p, r, \phi, \psi\}^T$$

There are 30 states associated with the actuators in x_{act}. The remaining states, x_ζ, are associated with the elastic and aerodynamics states, $x_\zeta = \{x_e, \dot{x}_e, x_{lag}\}^T$. The x_e and $\dot{x}_e$ vectors contain 14 states each, corresponding to the flexible body modes and x_{lag} contains 60 states corresponding to the lags due to unsteady aerodynamics. The resulting state space matrices are

$$\begin{bmatrix} \dot{x}_{AS} \\ \dot{x}_\zeta \\ \dot{x}_{act} \end{bmatrix} = \begin{bmatrix} A_{rr} & A_{re} & B_{rr} \\ A_{er} & A_{ee} & B_{re} \\ 0 & 0 & A_{act} \end{bmatrix} \begin{bmatrix} x_{AS} \\ x_\zeta \\ x_{act} \end{bmatrix} + \begin{bmatrix} 0 \\ 0 \\ B_{act} \end{bmatrix} u_{act}$$

The A_p matrix has special structure as seen in Figure 4. Knowledge of the location and meaning of the individual states are exploited in the following sections to construct a reduced order model for control design.
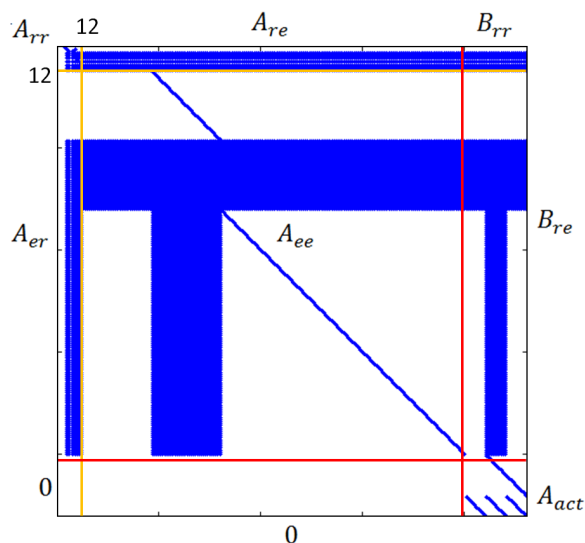
Figure 4. X-56A State-Space Model A_p Matrix

There are 10 control surfaces on the vehicle corresponding to five surfaces on each wing as seen in Figure 5. The five left wing actuators are labeled CSL-01, corresponding to the inner most surface, through CSL-05, the outer most surface. Correspondingly, the five right wing actuators are labeled CSR-01 through CSR-05. The rigid body state sensors are assumed to be at the center of gravity of the vehicle.

The six accelerometer locations are also shown in Figure 5. The two accelerometers on the center body are labeled ASESNSR100, at the front of the vehicle, and ASESNSR1000, at the rear of the vehicle. The outer most accelerometers on the left wing are labeled ASESNSR400 and ASESNSR600, while the outer most accelerometers on the right wing are labeled ASESNSR1100 and ASESNSR1300. The body (CSL-01, CSR-01) and outer most flaps (CSL-05, CSR-05) will be used for stabilization and damping augmentation on the vehicle. The sensors to be used for control include the roll (p), pitch (q) and yaw (r) rate sensors,
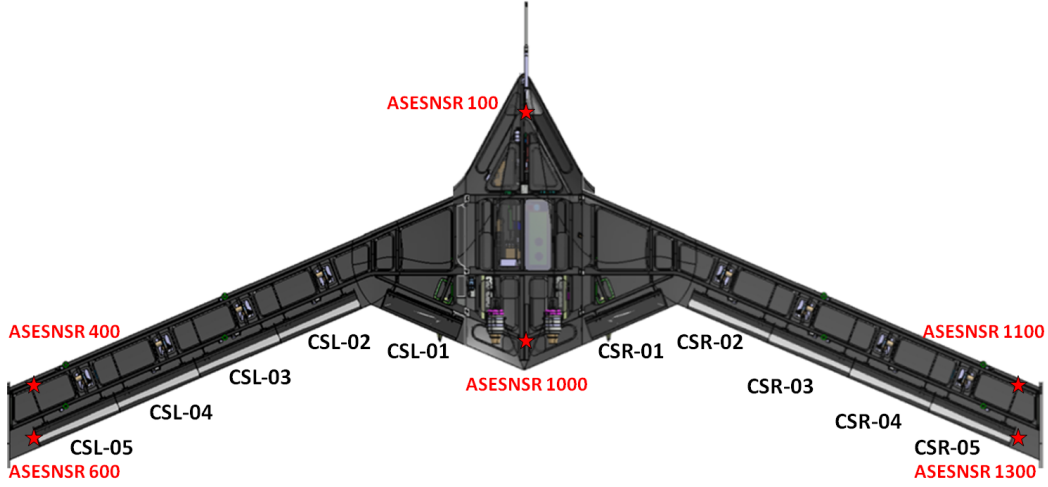
Figure 5. X-56A Sensor and Actuator Locations

the accelerometer at the trailing edge, body center (ASESNSR1000) and the accelerometers on the trailing edge at the outer most points (ASESNSR600, ASESNSR1300).

Classical model reduction techniques, truncation and residualization, will be applied to the structured, full order, 130 state, X-56A vehicle state space models. These techniques will be applied in sequential stages to reduce the state order. Balanced model reduction is applied to the resulting reduced order X-56A vehicle models. The following subsections describe the order reduction steps taken based on the structure of the state-space models.

IV.   X-56A Reduced Order Models

The objective of this section is to develop a reduced order, linear parameter-varying (LPV) model of the X-56A vehicle for control design. The full order X-56A LPV model has 130 states and is defined at 7 flight conditions, scheduled by normalized velocity V/V_{ref}. The states of the reduced order X-56A LPV model must retain the same meaning across flight conditions. The following sections describe the individual steps performed to eliminate states. A majority of the reduction steps are based on the physics of the given aeroelastic flight control system.

A.   Truncation and Residualization

Model reduction by truncation is preferred when accuracy at high frequencies is required. The truncated model G_r is equal to the full order model G at infinite frequency, $G(\infty) = G_r(\infty) = D$. For truncation, the state vector is partitioned into two components $\begin{bmatrix} x_1 & x_2 \end{bmatrix}^T$, where x_1 corresponds to the states to be kept and x_2 corresponds to the states to be eliminated. The corresponding A, B and C matrices are defined as

$$A = \begin{bmatrix} A_{11} & A_{12} \\ A_{21} & A_{22} \end{bmatrix}, \qquad B = \begin{bmatrix} B_1 \\ B_2 \end{bmatrix}, \qquad C = \begin{bmatrix} C_1 & C_2 \end{bmatrix},$$

The truncated model G_r is equivalent to

$$\begin{aligned} \dot{x}_1 &= A_{11}x_1 + B_1 u \\ y &= C_1 x_1 + Du \end{aligned}$$

Residualization preserves the steady state gain of a system, $G(0) = G_r(0)$, by setting the state derivatives of the states to be removed to zero. Hence, residualization leads to a more accurate representation of the

American Institute of Aeronautics and Astronautics

original system response at low frequency. As in truncation, the x_1 states are retained and the x_2 states are eliminated. The resulting residualized reduced order model, G_r is given by

$$
\begin{aligned}
\dot{x}_1 &= (A_{11} - A_{12}A_{22}^{-1}A_{21})x_1 &+& (B_1 - A_{12}A_{22}^{-1}B_2)u \\
y &= (C_1 - C_2 A_{22}^{-1}A_{21})x_1 &+& (D - C_2 A_{22}^{-1}B_2)u
\end{aligned}
$$

Truncation and residualization are used to construct reduced order models of the X-56A vehicle for controller synthesis to stabilize and augment damping of the uncontrolled vehicle.

B. Actuator State Reduction

The 130 state X-56A vehicle model includes 30 states associated with the actuators. There are 10, three state actuator models include in the state-space models. The same actuator model is used for all the surfaces. A Bode plot of the actuator model is shown in Figure 6.
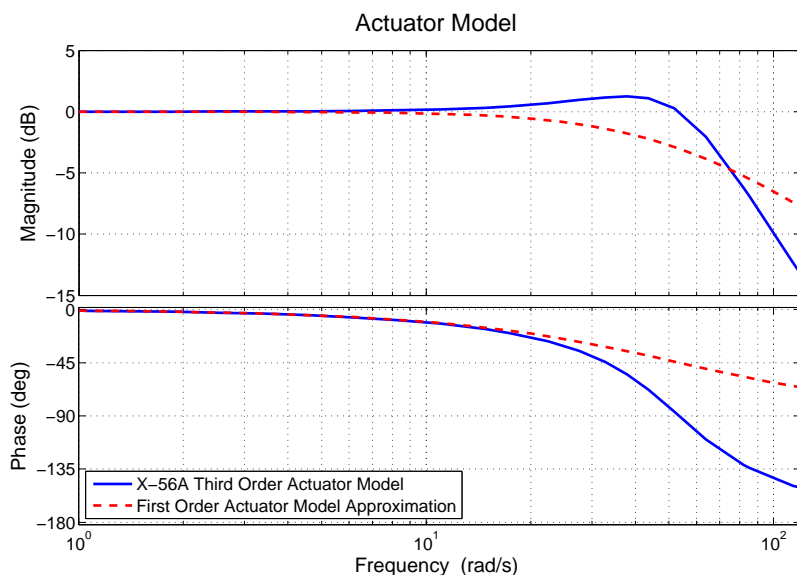
Figure 6. **X-56A Actuator Full and Reduced Order Bode Plots**

The first step to reduce the model order is to eliminate the actuator states from the X-56A vehicle models. The actuator models stand separate from the vehicle aeroelastic model as there is no direct coupling between the actuators and aeroelastic states. The full actuator dynamics, or a reduced order approximation of their dynamics, can be included in the control design if necessary. The elimination of the actuator models from the full order X-56A vehicle models eliminates 30 states from the full order X-56A vehicle model and allows the order reduction to focus on the aeroelastic states of the vehicle. Figure 7 provides a comparison between the full and reduced order X-56A models with the actuator states residualized. The reduced order X-56A models shown, should have the same dynamics as the full order models modulo the gain and phase variation due to the actuator models. Note that there is significant variation in the 20-80 rad/s frequency range between the two models at $V/V_{ref} = 0.58$ and $V/V_{ref} = 1$, for the transfer function between the left body flap and outermost wing surface, and the roll rate and outboard accelerometer. An accurate model of the X-56A in this frequency range is important as the three aeroelastic modes which become unstable range from 15 to 40 rad/s.

A first order approximation of the actuators models associated with the left and right body flaps, CSL-01 and CSR-01, is developed to address the discrepancy between the full and reduced order vehicle models.

American Institute of Aeronautics and Astronautics

Consider the three state, state-space description of the actuator model as provided by NASA Dryden.

$$\dot{x}_{act} = \begin{bmatrix} 0 & 1 & 0 \\ 0 & 0 & 1 \\ -a_{31} & -a_{21} & -a_{11} \end{bmatrix} x_{act} + \begin{bmatrix} 0 \\ 0 \\ a_{31} \end{bmatrix} u$$

$$y = \begin{bmatrix} 1 & 0 & 0 \end{bmatrix} x_{act} + Du$$

The MATLAB command `modred` is used to residualize the information in states 2 and 3 to generate an accurate, first order model at low frequency. Figure 6 shows a comparison of the Bode plots of the full order and first order actuator models.
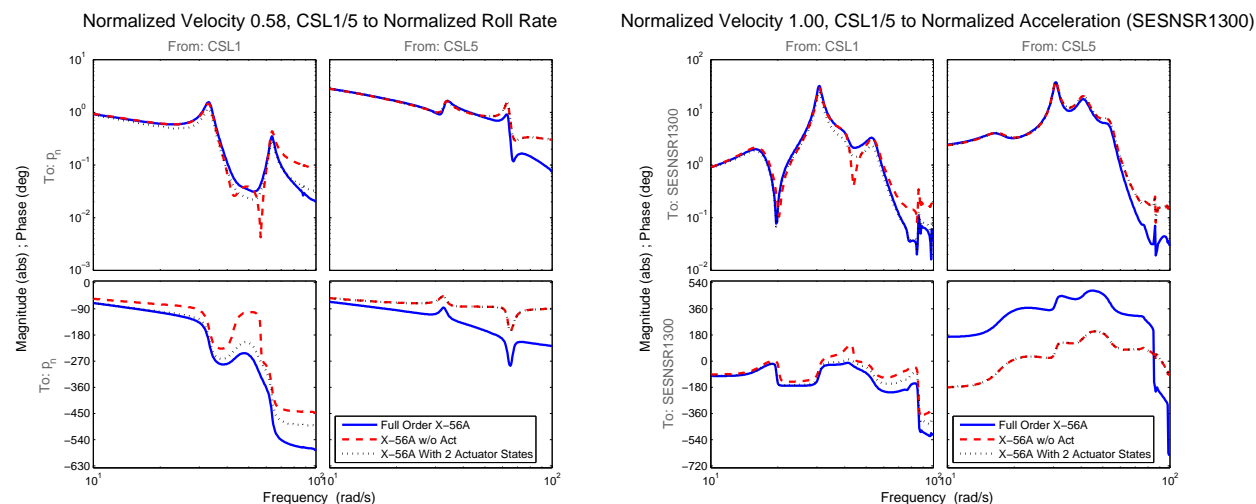
Figure 7. X-56A Full Order Model and Models with Actuators Removed

The phase characteristics of the first order actuator closely matches the full order actuator model up to 20 rad/s. Figure 7 shows that retaining 2 states of left and right body flap actuators, CSL-01 and CSR-01, significantly improves the response of the reduced order X-56A model. This model will be used for subsequent order reductions. Retaining states 101 and 106 in the state vector x, which correspond to actuators CSL-01 and CSR-01, leads to an improved match between the full and reduced order X-56A models as seen in Figure 7. The improved accuracy of the reduced order aeroelastic model in the frequency range 20-80 rad/s warrants retaining these extra two states. The resulting reduced order model has 102 states.

C. Unsteady Aerodynamic State Reduction

The full order X-56A contains 12 rigid body states, 14 flexible body modes, 30 actuator states and 60 aerodynamic lag states associated with the unsteady aerodynamics. The aerodynamic lag states correspond to states 41 through 100 in the full order state space description (see Figure 4). There are three lag states at 17.6, 70.3 and 158 rad/s, for each rigid body and flexible mode.

The full order 130 state X-56A model was approximated in the previous section by a 102 state reduced order model, in which 28 actuator states were removed while retaining 2 states associated with actuators CSL-01 and CSR-01. The objective of this section is to construct a reduced order model which closely approximates the 102 state X-56A by eliminating unneeded states associated with the unsteady aerodynamics. It was found that retaining states 41, 42, 46, 47, 48, 53, 54, 59, 65 led to an accurate low order models which retained the correct unstable modes of the original system. States 41, 47, 53, 59 and 65 correspond to the low frequency first order lag at 17.6 rad/s, states 42, 48, and 54 correspond to the middle frequency first order lag at 70.3 rad/s, and state 46 corresponds to the high frequency first order lag at 158 rad/s.

Residualization is used to eliminate states 43-45, 49-52, 55-58, 60-64 and 66-100. Figure 8 provides a comparison between the reduced order models with 51 aerodynamic lag states residualized and the reduced order models with 102 states. The reduced order X-56A models with 51 aerodynamic lag states residualized

American Institute of Aeronautics and Astronautics

have the same dynamics as the higher order models. The reduced order model captures the dynamic characteristics of the high order model well in the 20-80 rad/s frequency range for the transfer functions between the left body flap and outermost wing surface, and the pitch rate (q) and left wing outboard accelerometer (ASESNSR 600). The resulting reduced order model has 51 states.
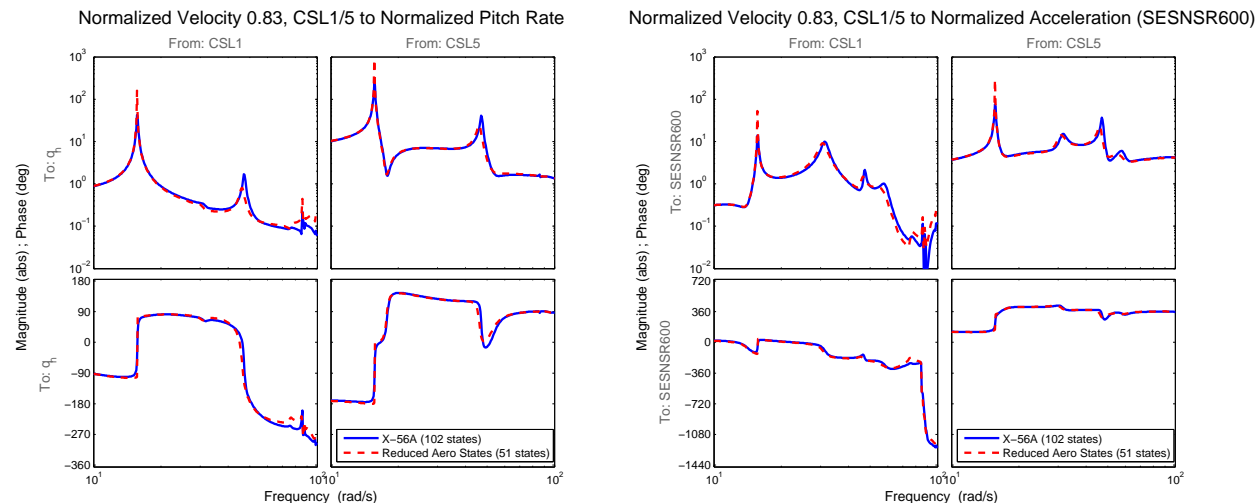
Figure 8. X-56A Reduced Order Model (102 states) and Model with 51 Aerodynamic Lag States Residualized (51 states)

D. Rigid Body State Truncation

The 12 rigid body states are part of the 51 state, reduce order model of the X-56A vehicle constructed in the previous section. Recall, these are the first 12 states of the X-56A models and correspond to $x, h, \theta, u, \alpha, q, y, \beta, p, r, \phi,$ and ψ. The physics of the model allow elimination of position (x, h, y), velocity (u) and angular $(\theta, \beta, \phi, \psi)$ states as they do not play a role in the aeroelastic dynamics to be controlled using this model. Recall the objective is to develop reduced order models, with consistent states across the flight envelope, for stabilization and damping augmentation using feedback control. States α, q, p, and r are retained. State truncation is used to eliminate the x, h, y, u, θ, β, ϕ, and ψ states resulting in a 43 state reduced order model.

Bode plots of the transfer functions between the left body flap and outermost wing surface, and the pitch rate and left wing outboard accelerometer at $V/V_{ref} = 0.83$ are shown in Figure 9. The resulting reduced order models have 43 states and accurately match the higher order models across the flight envelope.

E. Flexible Body State Truncation

The reduced order X-56A model with 43 states retains all 14 flexible body modes in the original full order X-56A vehicle model. The states that describe these modes correspond to the modal displacements (states 13-26) and modal velocities (states 27-40) in the original state-space A matrix. Since eight rigid body states were removed, the flexible body modes in the reduced order model correspond to states 5-32 in the 43 state, reduced order model. The flexible mode states are ordered in increasing model frequencies from 19.87 to 119.35 rad/s. Since the X-56A reduce order model will be used for control design, the model needs to capture the vehicle dynamics accurately between 10 and 80 rad/s, which includes the 3 flexible modes which become unstable. Hence, given the restricted bandwidth of the control system, only the first four flexible body modes up to 62.4 rad/s are retained in the reduced order model.

The fifth through fourteenth flexible modes are truncated from the 43 state reduced order X-56A model generated in the previous section. Bode plots of the transfer functions between the left body flap and outermost wing surface, and the pitch rate and left wing outboard accelerometer at $V/V_{ref} = 0.83$ are shown in Figure 10. The resulting reduced order model has 23 states. The reduced order model matches the higher order model accurately across the flight envelope and correctly retains the stability characteristics of models

American Institute of Aeronautics and Astronautics
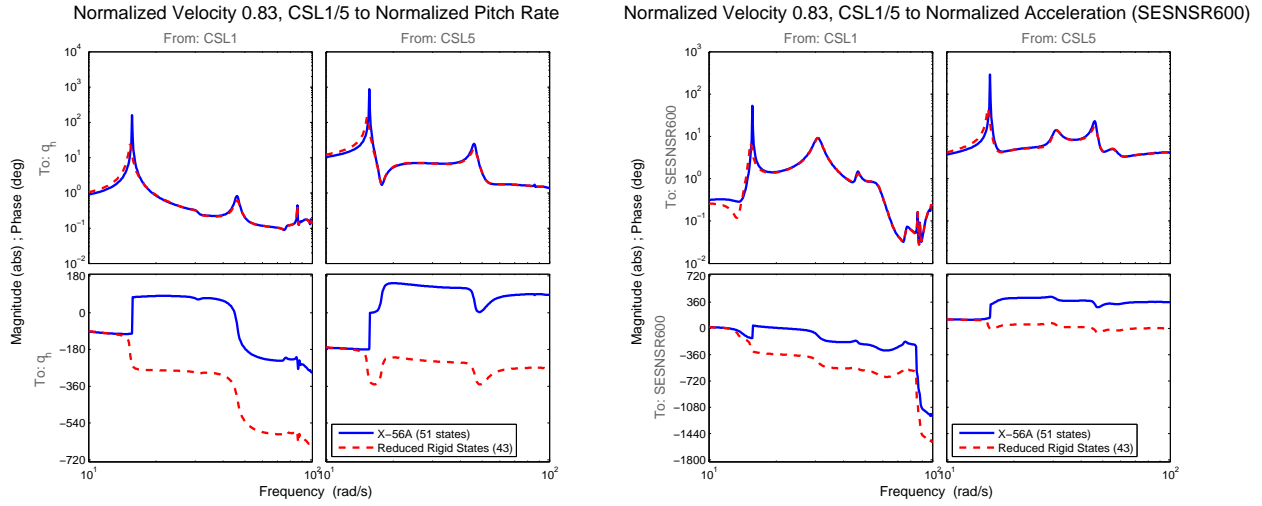
Figure 9. X-56A Reduced Order Model (51 states) with Rigid Body States Truncated (43 states)

as well. The match between these models breaks down above 70 rad/s due to the elimination of the higher frequency flexible body modes.
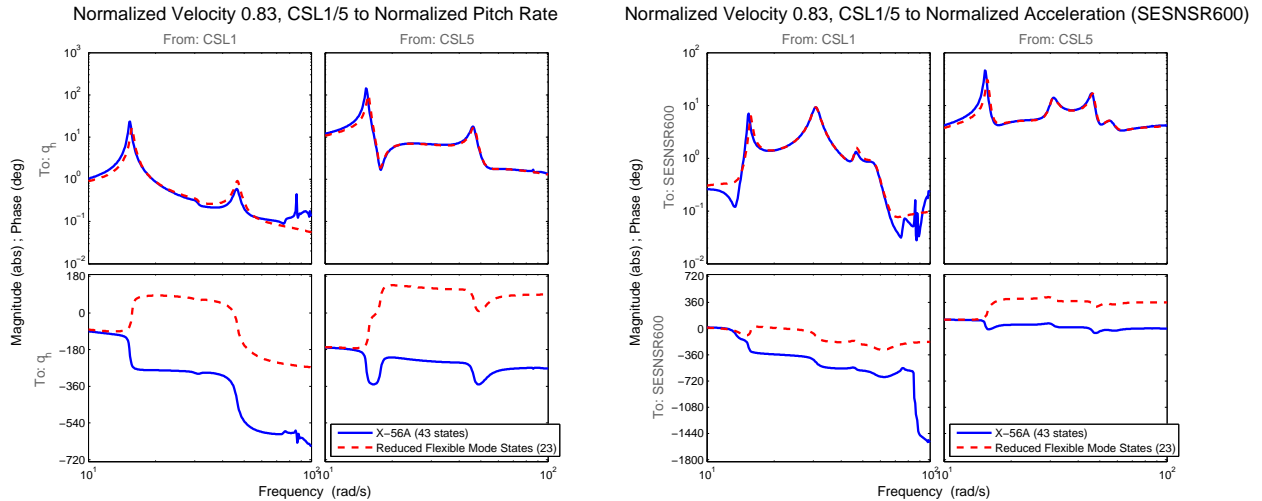
Figure 10. X-56A Reduced Order Model (43 states) versus Flexible Body States Truncated (23 states)

F. Balanced Realization Residualization

The reduced order, 23 state, X-56A vehicle model at each flight condition has been generated from the full order, 130 state, model using truncation and residualization techniques. The reduction techniques work into the original coordinate system, hence the meaning of the retained states are consistent across flight condition and the same as in the full order model. The objective of this section is to use balanced realization, a multivariable model reduction technique, to further reduce the order of the X-56A models across the flight envelope. The key is that all models must retain the same meaning of the transformed state at each flight condition. To enforce this requirement, the same constant transformation will be applied to every model in the model set.

Note that for control design all input/output pairs of the models are important. A priori it is difficult to know which input/output pairs are key to synthesizing a robust, high performing controller. Hence at

American Institute of Aeronautics and Astronautics

this point in model development, an accurate model for all input/output pairs should be developed. The balanced realization technique transforms the original model into a balanced controllable/observable form and the states that are least controllable and observable are eliminated. The gain from each input to output influences the overall controllability/observability transformation. The X-56A inputs have different control authority due to their location on the vehicle, i.e the body flaps (CSL-01 and CSR-01) are less effective than the outboard flaps (CSL-05 and CSR-05). Similarly the sensor measurements have different sensitivities and of different units (rates versus accelerations). To balance the equal importance of channels, the 23 state reduced order model input/output channels are scaled. The inputs, CSL-01, CSR-01, CSL-05, and CSR-05, are scaled with $\mathrm{diag}(1, 1, 0.1, 0.1)$. The outputs, p, q, r, ASENSR1000, ASENSR600 and ASENSR1300, are scaled with $\mathrm{diag}(2, 50, 20, 0.01, 0.01, 0.01)$. Hence each model is scaled as

$$
\mathrm{x56a\_red2(i)} =
\begin{bmatrix}
2 & 0 & 0 & 0 & 0 & 0 \\
0 & 50 & 0 & 0 & 0 & 0 \\
0 & 0 & 20 & 0 & 0 & 0 \\
0 & 0 & 0 & 0.01 & 0 & 0 \\
0 & 0 & 0 & 0 & 0.01 & 0 \\
0 & 0 & 0 & 0 & 0 & 0.01
\end{bmatrix}
\cdot \mathrm{x56a\_red(i)} \cdot
\begin{bmatrix}
1 & 0 & 0 & 0 \\
0 & 1 & 0 & 0 \\
0 & 0 & 0.1 & 0 \\
0 & 0 & 0 & 0.1
\end{bmatrix}
$$

prior to applying the balanced transformation.

A single balanced transformation is applied to all the 23 state reduced order models. The states of the transformed models all have the same meaning, though the meaning of the states are different from meaning of the original model's states. It was determined through trial and error that the best transformation was associated with the X-56A model at $V/V_{ref} = 0.83$. After this transformation is applied to all the models, the 8 states with the smallest controllability and observability singular values are truncated from each model.

Bode plots of the transfer functions between the left body flap and outermost wing surface, and the pitch rate (q) and left wing outboard accelerometer at $V/V_{ref} = 0.83$ and $V/V_{ref} = 1$ are shown in Figure 11. The resulting reduced order models have 15 states. The reduced order models match the higher order models very accurately across the flight envelope and correctly retain the stability characteristics of these models. Each reduced order model at flight conditions $V/V_{ref} = 0.58$ to $V/V_{ref} = 1.08$ has 4 actuator inputs, 6 sensor measurements and 15 states.
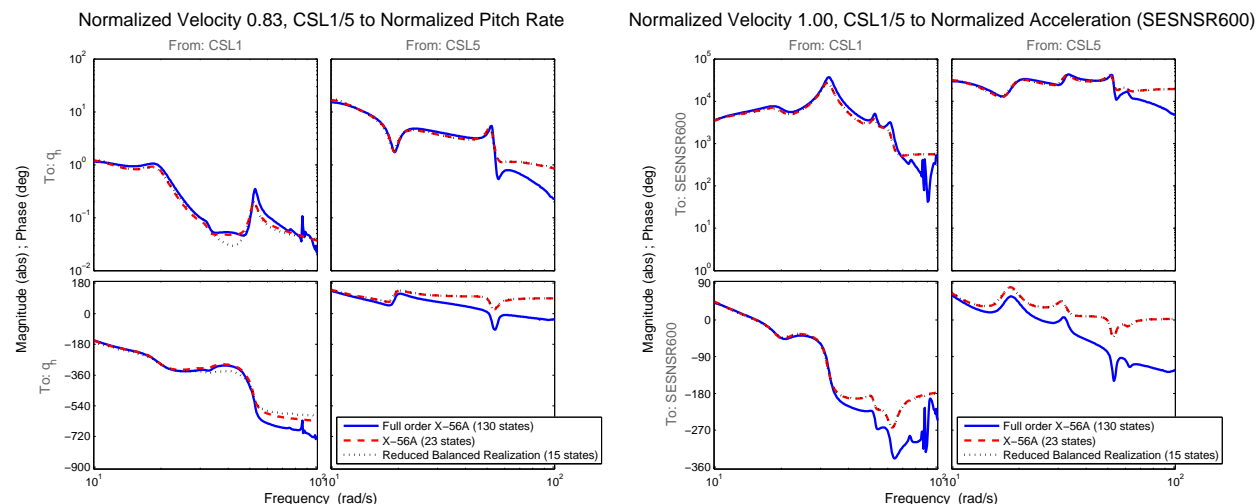
Figure 11. X-56A Reduced Order Model (23 states) Versus Balanced Residualization States Truncated (15 states)

American Institute of Aeronautics and Astronautics

V. X-56A Stabilization and Damping Augmentation

The control objective for the X-56A is to stabilize the vehicle across its flight envelope, $V/V_{ref} = 0.58$ to $V/V_{ref} = 1.08$, and augment the damping of the four aeroelastic modes between 10 and 45 rad/s. The body freedom flutter mode of the X-56A linearized models become unstable at $V/V_{ref} = 0.83$, the first symmetric bending becomes unstable at $V/V_{ref} = 0.92$ and the first anti-symmetric goes unstable at $V/V_{ref} = 1$. The feedback measurements for control are the body rates, p, q, r, the center body accelerometer at the trailing edge (ASENSR1000), and the two accelerometers at the trailing edge wing tips (ASENSR600, ASENSR1300). The reduced order, 15 state model of the X-56A at each flight condition is used for control design. The following sections present the H_∞ controllers synthesized at each operating, e.g. $V/V_{ref} = 0.58$, $V/V_{ref} = 0.67$, and a single, rate-bound LPV controller synthesized to work across the flight envelope.

A. H_∞ Point Control Design

The stabilization and damping augmentation control design objectives are posed as a standard weighted H_∞ error minimization problem as seen in Figure 12.
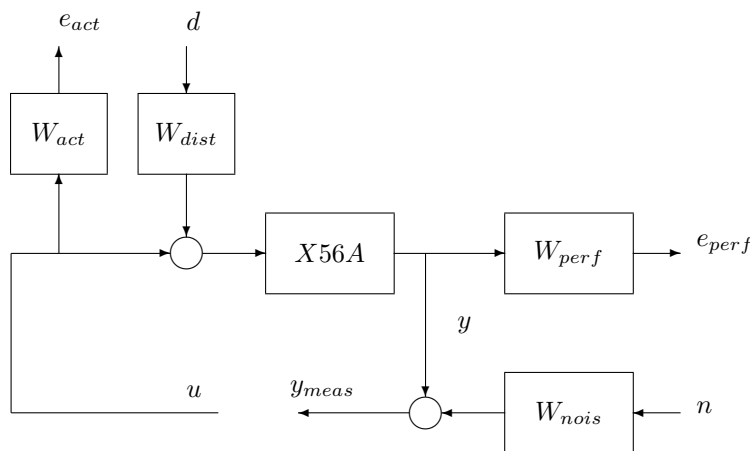
Figure 12. X-56A Stabilization and Damping Augmentation Controller Interconnection

The open-loop control design interconnection, Figure 12, has a disturbance, d, entering at the actuator inputs and the sensor noise augmenting the feedback measurements. The input weights, W_{dist} and W_{nois}, are scaled to reflect the gain of the individual actuators and the response levels of the rates and acceleration. The weight W_{dist} is selected to be $2 \cdot I_{4\times4}$. The noise on the rate sensors, p, q, r, is selected to be $W_{pqrnois} = \frac{0.2}{57.3}I_{3\times3}$ and the noise on the acecelerometers is modeled as $W_{accnois} = 0.01 \cdot I_{3\times3}$. Hence the W_{nois} weight is $\mathrm{diag}(W_{pqrnois}, W_{accnois})$.

Two sets of signals are penalized in the control design: control commands u, and rate and acceleration outputs. The control commands are penalized with weight W_{act} which corresponds to $0.5 \cdot I_{4\times4}$, the control commands are in radians. Each control command is penalized equally since all the surfaces have the same deflection limits. W_{perf} penalizes the vehicle rates and accelerations to augment the vehicle damping. The weights are adjusted to account for the different transfer gains in the system. Roll rate, p, weight is a constant 0.02 and the pitch rate weight is 0.4. The yaw rate r is not included in the performance objective since there is sufficient damping already present in this channel. Hence its weight is 0. The three accelerometer performance signals are weighted with 0.06, hence the performance weighting function is defined as $W_{perf} = \mathrm{diag}(0.02, 0.4, 0, 0.06 \cdot I_{3\times3})$.

The point design, H_∞ controllers for the control interconnection in Figure 12 are synthesized at the seven flight conditions $V/V_{ref} = 0.58$, $V/V_{ref} = 0.67$, $V/V_{ref} = 0.75$, $V/V_{ref} = 0.83$, $V/V_{ref} = 0.92$, $V/V_{ref} = 1$, and $V/V_{ref} = 1.08$. The point design closed-loop systems achieve an H_∞ norm between 1.00 and 1.01. Hence the weighting functions lead to similar performance of the damping augmentation controllers across the flight envelope. Each point design is stable and significantly attenuates the disturbance responses across the flight envelope. Note that the plant model used in the analysis is the same as used for design.

Figure 13 show a comparison of the open-loop and closed-loop frequency responses of an input disturbance entering in the left body flap channel, to roll rate (p), and the left wing, trailing edge accelerometer. Similar levels of performance is achieved from the other disturbance inputs to the rate and acceleration responses. The magnitude frequency response of the channel 1 disturbance (disturbance to CSL-01) to left wing outer actuator is shown in Figure 14. Note that the actuator is modeled as unity gain in this setup. The closed-loop bandwidth at two flight conditions exceeds several hundred radians/sec. This would imply high frequency disturbances would be observed at the output of the actuators. The actual control system has actuators that roll off at 40 rad/s which would mitigate this high bandwidth issue.
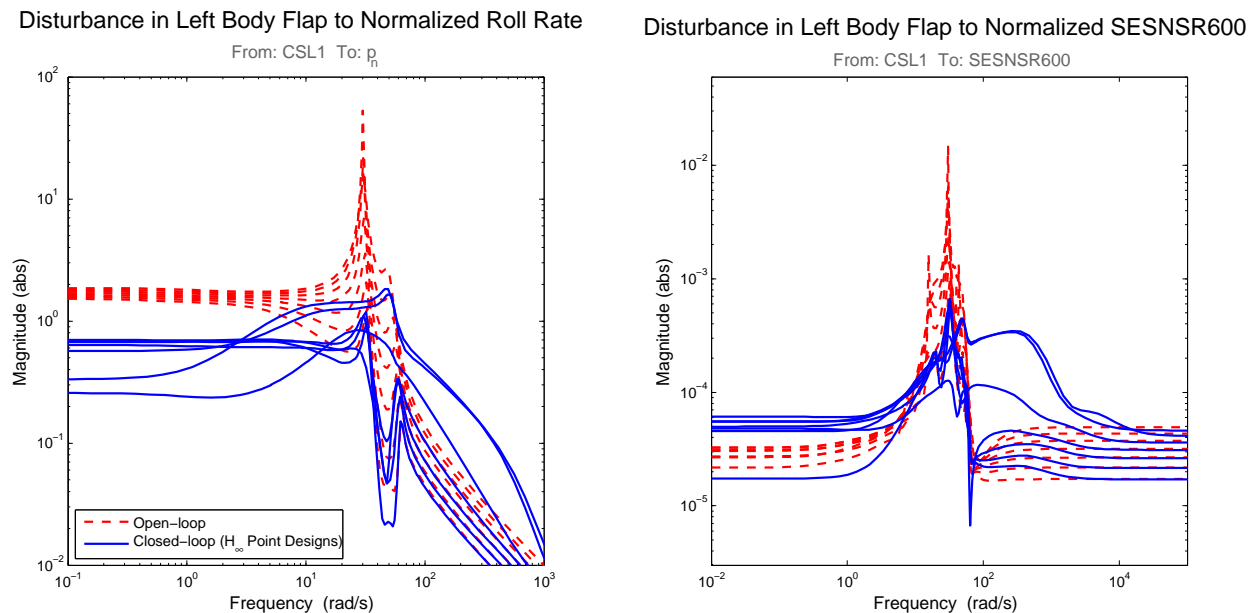
Figure 13. Open vs Closed-loop X-56A H_∞ Controller: $d \to p$, $d \to$ ASENSR600 (Frequency response for all 7 Point Designs)

Consider a doublet input disturbance to the left, inboard body flap (CSL-01). The open-loop and closed-loop responses of the vehicle at the $V/V_{ref} = 0.75$ and $V/V_{ref} = 1$ flight conditions are shown in Figure 15. Sensor noise is included on the feedback measurements. Figure 16 shows the control commands generated by the controllers to attenuate the disturbances. Note that the plant model used in simulation is the same that was used in design, and the actuator is modeled as unity gain. Time response plots of the open-loop versus closed-loop system with the H_∞ point design controllers implemented show a similar story to the frequency domain results.

The high loop bandwidth controllers at the two flight conditions results in the accelerometer noise driving the actuator surfaces. This would be unacceptable in the final design. The inclusion of the actuator models in the design process would mitigate these effects. These initial H_∞ point design controllers indicate that the stabilization and damping augmentation objectives are obtainable at each point in the flight envelope.

B. Rate-Bounded LPV Control Design

The stabilization and damping augmentation control design objectives are posed as a LPV error minimization problem as seen in Figure 17. The LPV control design objective is to synthesize a single, LPV controller which automatically schedules across the flight envelope. Velocity is the scheduled variable. Our focus is on rate-bounded LPV control designs.

The open-loop LPV control design interconnection, Figure 17, has a disturbance, d, entering at the actuator inputs and the sensor noise augmenting the feedback measurements. The control problem formulation is the same as for the H_∞ point designs as are the weighting functions W_{dist}, W_{nois}, W_{perf} and W_{act}. A single LPV controller is synthesized to stabilize and augment damping for the seven flight conditions $V/V_{ref} = 0.58$, $V/V_{ref} = 0.67$, $V/V_{ref} = 0.75$, $V/V_{ref} = 0.83$, $V/V_{ref} = 0.92$, $V/V_{ref} = 1$, and $V/V_{ref} = 1.08$. The rate

American Institute of Aeronautics and Astronautics
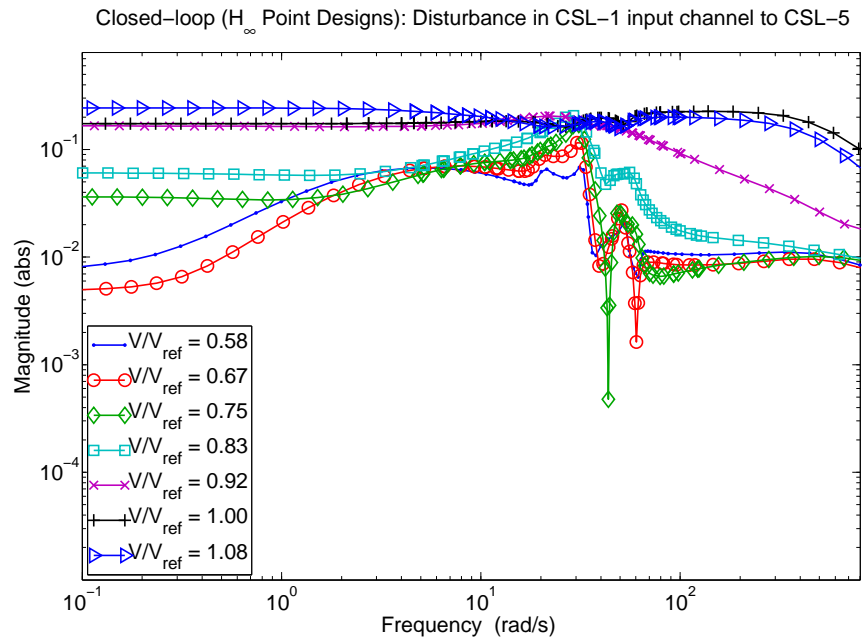
Figure 14. X-56A H_∞ Controller: $d \rightarrow$ CSL-05 (Frequency response for all 7 Point Designs)
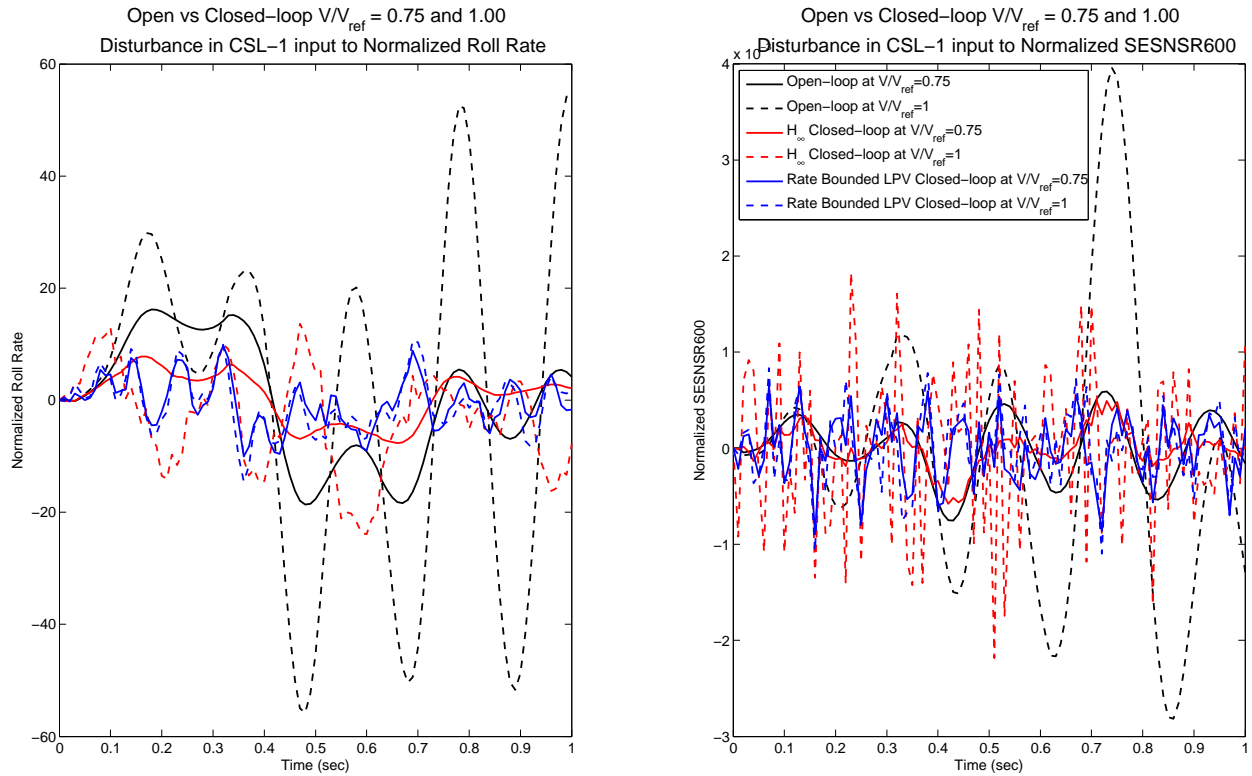
Figure 15. X-56A H_∞ and Rate-Bounded LPV Controller: $d \rightarrow p$, $d \rightarrow$ ASENSR600

of variation of the normalized velocity, the scheduling parameter, is assumed to be 0.0021/sec. Constraints on the rate of variation of velocity in the LPV control design are included via basis functions. A constant

American Institute of Aeronautics and Astronautics
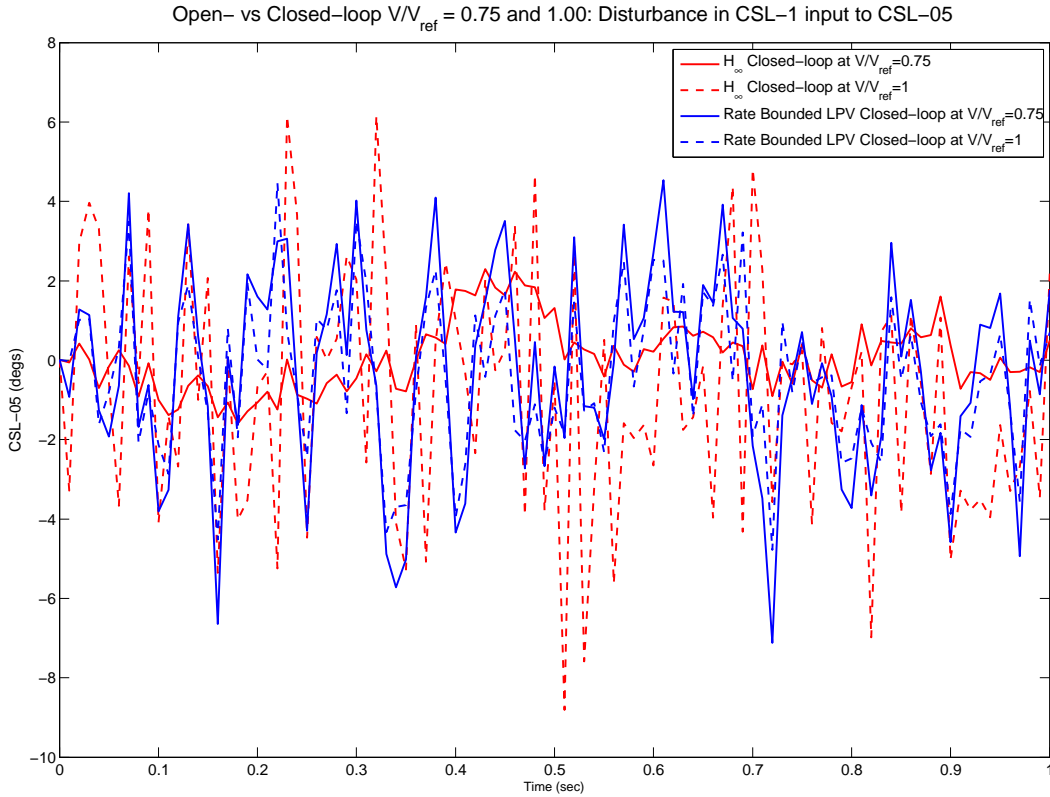
Figure 16. X-56A H_∞ and Rate-Bounded LPV Controller: $d \rightarrow$ CSL-05

and linear in velocity basis function are used in the LPV control design algorithms. The rate-bounded LPV controller achieves a closed-loop LPV norm of 1.20. This is very close to the H_∞ norm, 1, achieved by the point design. The LPV controllers is able to recover performance close to that of the point design controllers.

Figure 18 shows a comparison of the open-loop and closed-loop frequency responses of a disturbance entering in the left body flap (CSL-1) input channel to roll rate at each flight condition with the LPV rate-bounded controller. Each point design is stable and significantly attenuates the disturbance responses across the flight envelope. Note the plant model used in the analysis is the same as used for design. Figure 18 also shows a comparison of the open-loop and closed-loop frequency responses of the left body flap input disturbance to the left wing, trailing edge accelerometer. Similar levels of performance is achieved from the other disturbance inputs to the rate and acceleration responses.

The magnitude frequency response of the left body flap (CSL-1) input channel disturbance to left wing outer actuator is shown in Figure 19. Note that the actuator is modeled as unity gain in this setup. The closed-loop bandwidth for all the point designs start rolling off at approximately $100 \, \text{rad/s}$. Note that the bandwidth of the LPV rate-bounded design at each operating point is similar to the H_∞ point design controllers, Figure 14.

The performance of the LPV controller is studied in time-domain simulations. The same doublet input disturbance is used to excite the left, inboard body flap (CSL-01) as in the H_∞ closed-loop simulations. The open-loop and closed-loop responses of the vehicle at the $V/V_{ref} = 0.75$ and $V/V_{ref} = 1$ flight conditions are shown in Figure 15. Figure 16 shows the control commands generated by the LPV controller to attenuate the disturbances. The actuator is modeled as unity gain. The closed-loop bandwidth with the LPV controller implemented indicate that the accelerometer noise is driving the actuator surfaces. This would be unacceptable in the final design. The inclusion of the actuator models in the design process would mitigate these effects. This initial LPV controller indicates that the stabilization and damping augmentation objectives are obtainable at each point in the flight envelope.

American Institute of Aeronautics and Astronautics
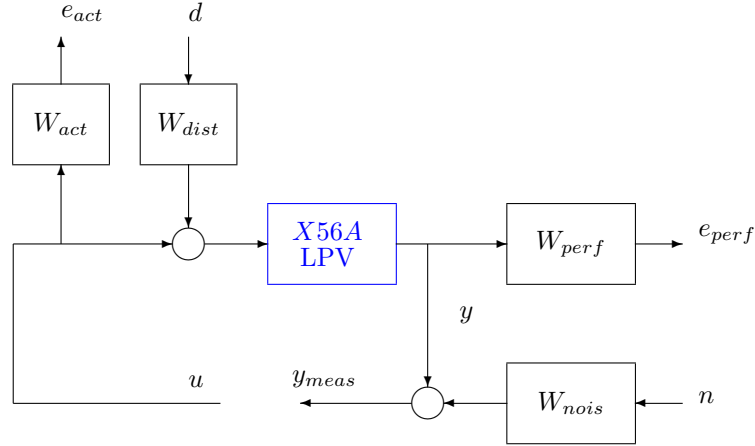
Figure 17. X-56A Stabilization and Damping Augmentation Controller Interconnection
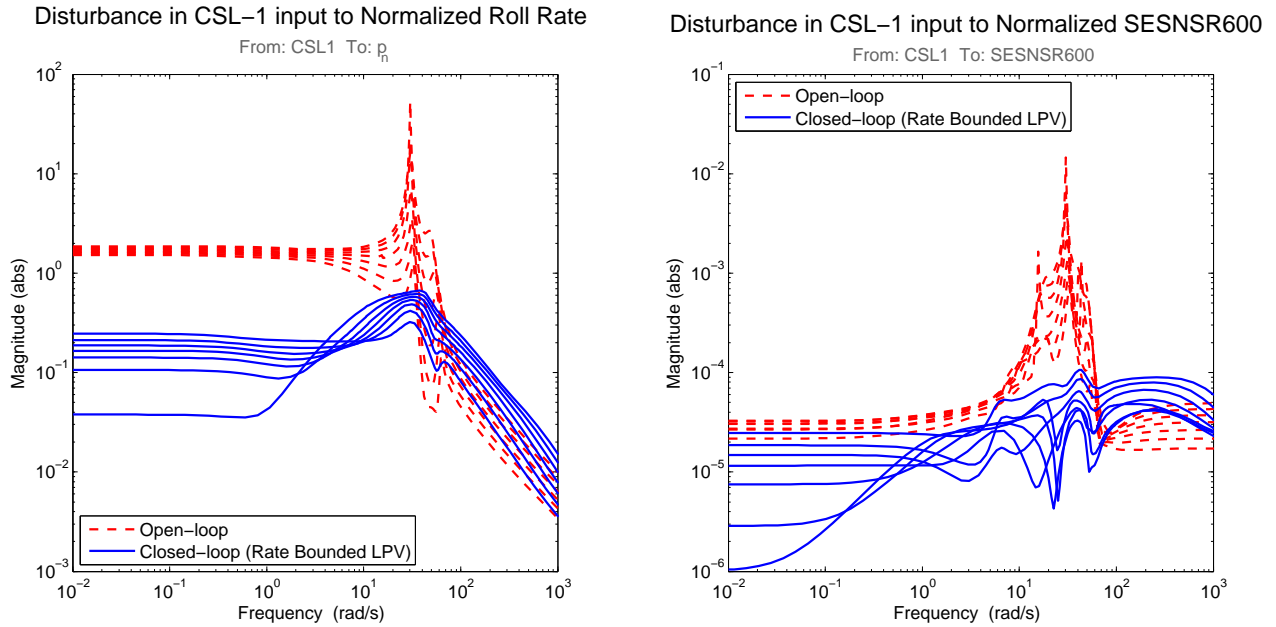
Figure 18. X-56A LPV Controller: $d \to p$, $d \to$ **ASENSR600**

C. Inclusion of Actuator Model in Control Design

A first order actuator mode is added to the X-56 A control design problem formulation as seen in Figure 20. The control design objectives are the same as in the previous section for the H_∞ point design and LPV controllers.

The first order actuator model, described in Section B, is $53.5/(s + 53.5)$. There are four actuators associated with the four X-56A surfaces used for control. In the interconnection shown in Figure 20, the four rate outputs of ACT, $\dot{\delta}$, and the four actuator displacements, δ, are input to the W_{act} weight. W_{act} is chosen as $W_{act} = \text{diag}(0.5 \cdot I_{4\times4}, 0.4 \cdot I_{4\times4})$. Inclusion of the actuator rate inputs provides a means of penalizing the high frequency content of the control commands, u.

Several weighting functions are modified due to the inclusion of the actuator models. The disturbance weight, W_{dist}, is taken to be $\dfrac{10}{s + 20} I_{4\times4}$ and the noise on the accelerometers is increased by a factor of 10. Otherwise the weighting functions are the same as the were in the original H_∞ point designs and LPV

American Institute of Aeronautics and Astronautics
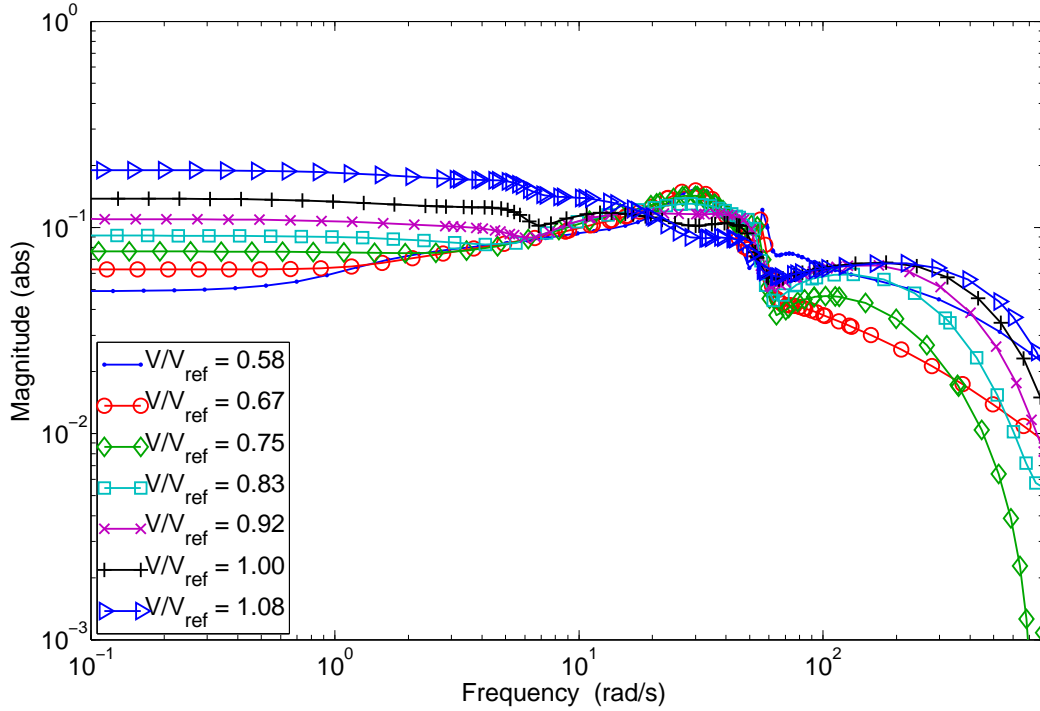
Figure 19. X-56A LPV Controller: $d \rightarrow$ **CSL-05**

control design. The rate of variation of the velocity, the scheduling parameter, in the LPV design is assumed to be 0.0167/sec. Constraints on the rate of variation of velocity in the LPV control design are included via basis functions. A constant and linear in velocity basis function are used in the LPV control design algorithms. The rate-bounded LPV controller achieves a closed-loop LPV norm of 1.20. The resulting H_∞ and LPV controllers have 23 states, 4 outputs and 6 inputs.

Figures 21 and 22 show a comparison of the open-loop and closed-loop frequency responses of a disturbance entering in the left body flap input channel, to roll rate and left wing trailing edge accelerometer at each flight condition. Each point design is stable and significantly attenuates the disturbance responses across the flight envelope. Note that the gain-scheduled LPV design nearly recovers the performance at the H_∞ point designs. This is important as it allows tailoring of the robustness and performance objectives for the individual point design prior to synthesizing a single, LPV controller.

The same doublet input disturbance is used to excite the left, inboard body flap (CSL-01) as in the original H_∞ and LPV closed-loop simulations in Sections A and B. The magnitude of the white noise on the p, q, r sensors was selected to be 0.2 deg/s and for the accelerometers it was selected to be 0.025 g. The open-loop and closed-loop responses of the vehicle at the $V/V_{ref} = 0.75$ and $V/V_{ref} = 1$ flight conditions are shown in Figure 23. Figure 24 shows that the control commands nicely attenuate the disturbances. Recall actuator is modeled as a first order system, $\dfrac{53.5}{s + 53.5}$. The closed-loop bandwidth with the LPV controller implemented indicate that the effect of accelerometer noise on the actuator surfaces is reduced as compared with previous designs

D. Full Order X-56A Control Design

The H_∞ and LPV controllers were implemented and tested with the full order X-56A model. The full order X-56A models have 130 states, 30 states associated with the actuators and 100 states associated with the aeroelastic modes of the vehicle. Figures 25 and 26 show a comparison of the open-loop and closed-loop frequency responses of a disturbance entering in the left body flap input channel, to roll rate and left wing,

American Institute of Aeronautics and Astronautics
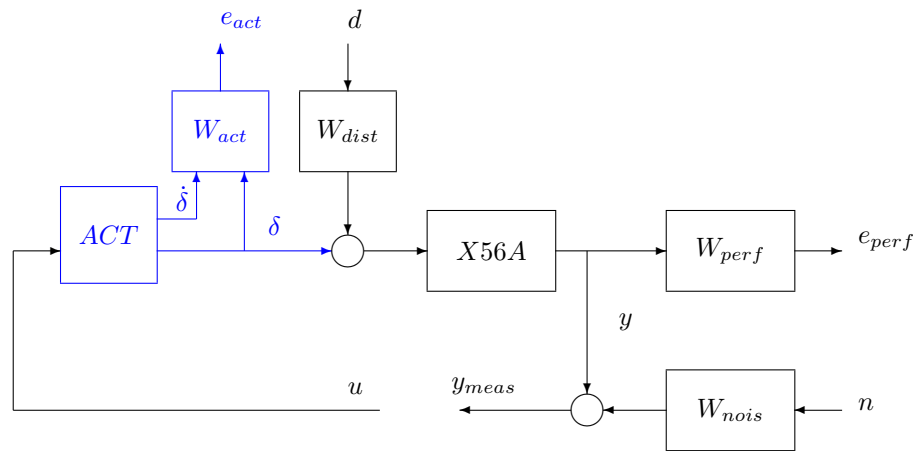
Figure 20. X-56A Control Design Interconnection with Actuator Model
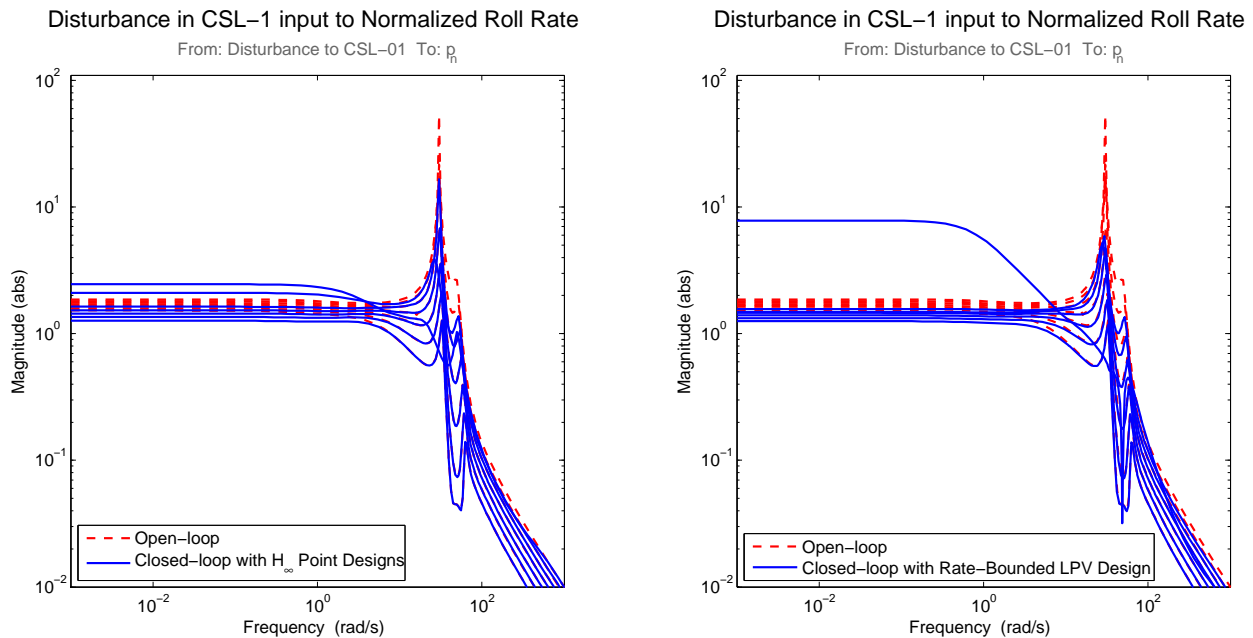
Figure 21. X-56A H_∞ Point Design and LPV Controller: $d \to p$

trailing edge accelerometer at each flight condition. The responses are similar when implemented with the reduced order X-56A models (Figures 21 and 22).

The open-loop and closed-loop time responses with the full order X-56A models at the $V/V_{ref} = 0.75$ and $V/V_{ref} = 1$ flight conditions are shown in Figures 27 and 28. The performance closely matches the responses of the closed-loop simulations with the reduced order X-56A model implemented (Figures 23 and 24). Hence the reduced order X-56A models with a first order actuator model accurately approximates the full order system for control design.

American Institute of Aeronautics and Astronautics
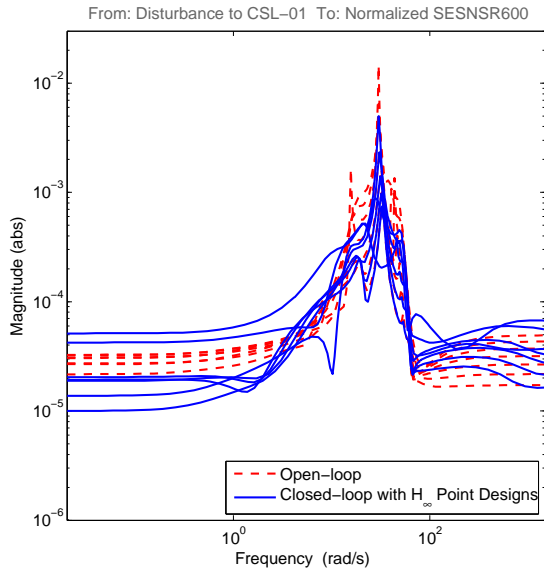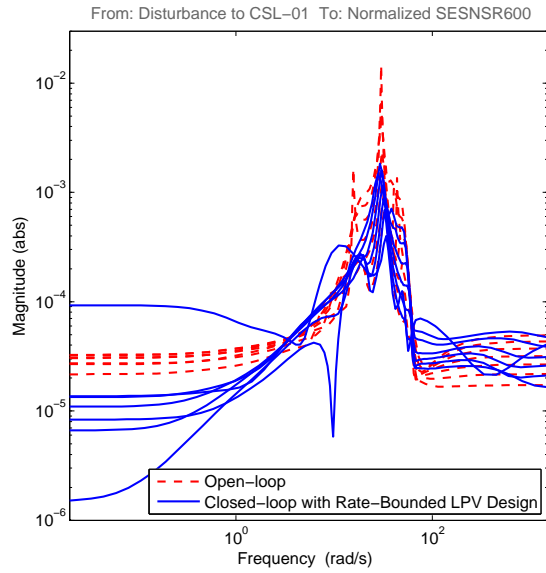
Figure 22. X-56A H_∞ Point Design and LPV Controller: $d \to$ ASENSR600
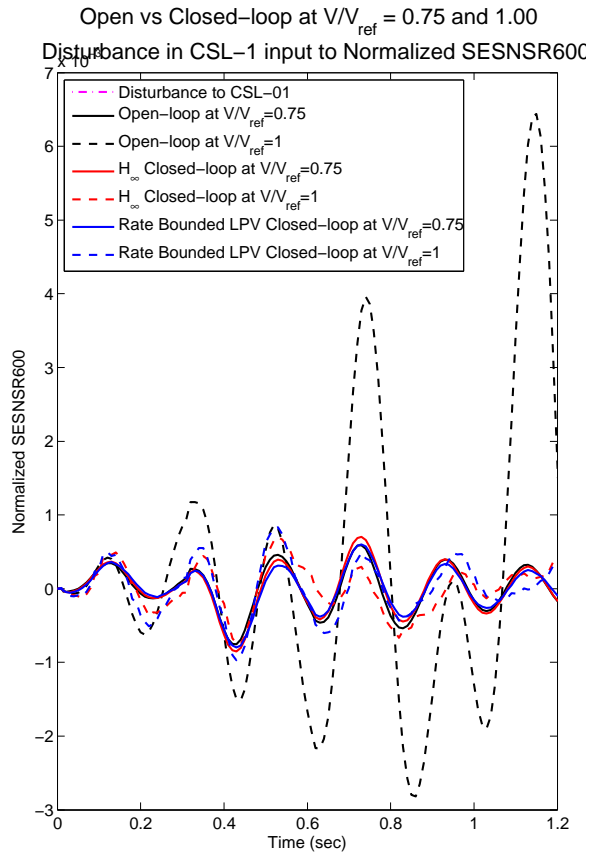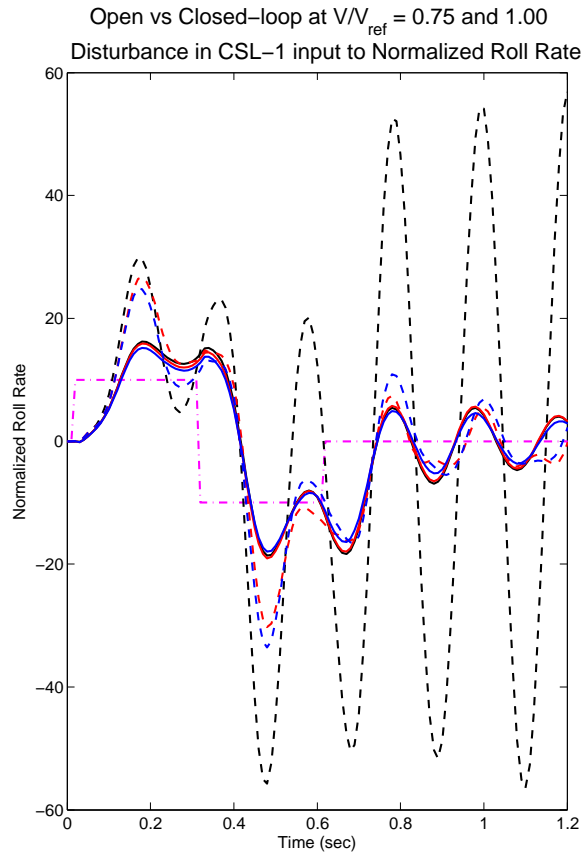
Figure 23. Open-Loop vs Closed-Loop X-56A with H_∞ and LPV Controllers and Actuators: $d \to p$, $d \to$ ASENSR600
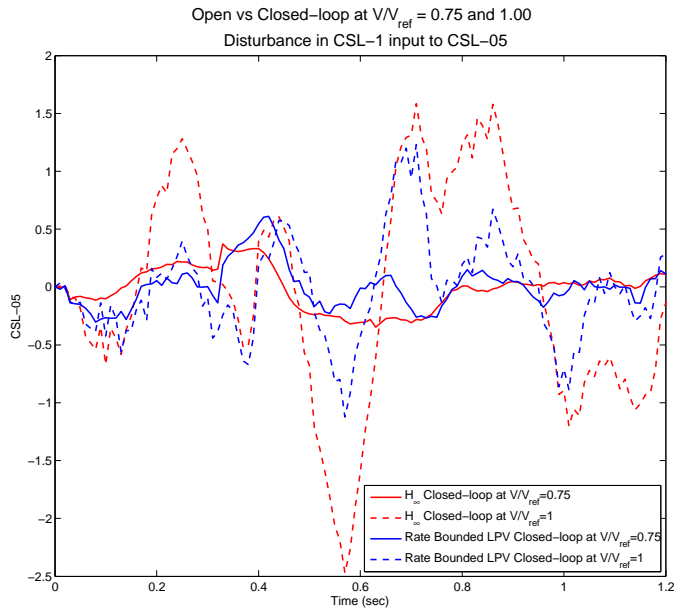
Figure 24. X-56A H_∞ and LPV Controllers with Actuators: $d \to$ CSL-05
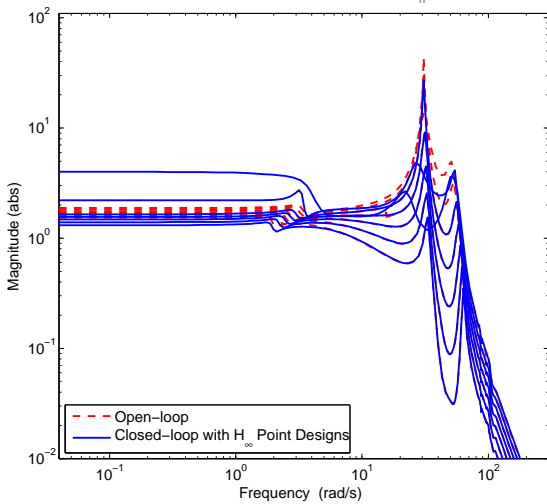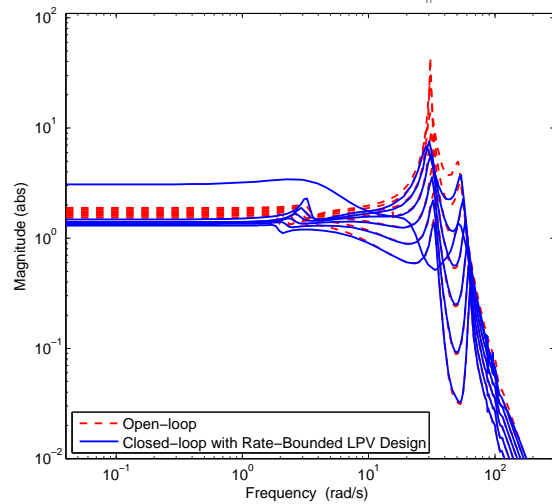
Figure 25. X-56A H_∞ Point Design and LPV Controller: Full Order X-56 Model, $d \to p$
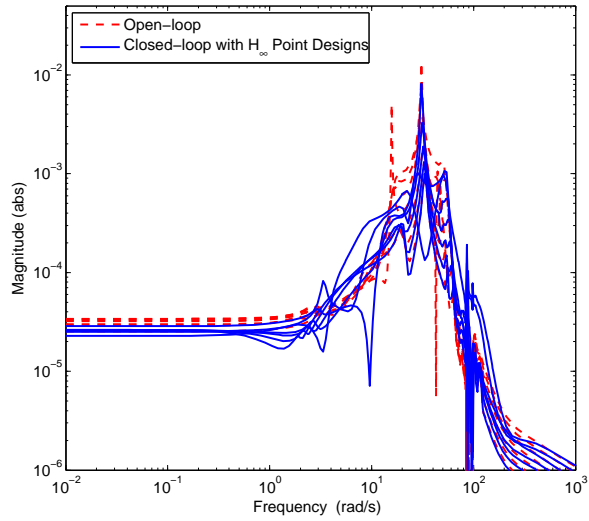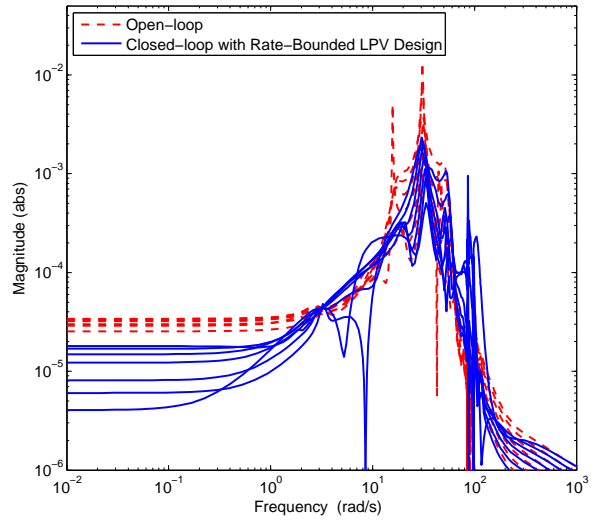
Figure 26. X-56A H_∞ Point Design and LPV Controller: Full Order X-56 Model, $d \rightarrow$ ASENSR600
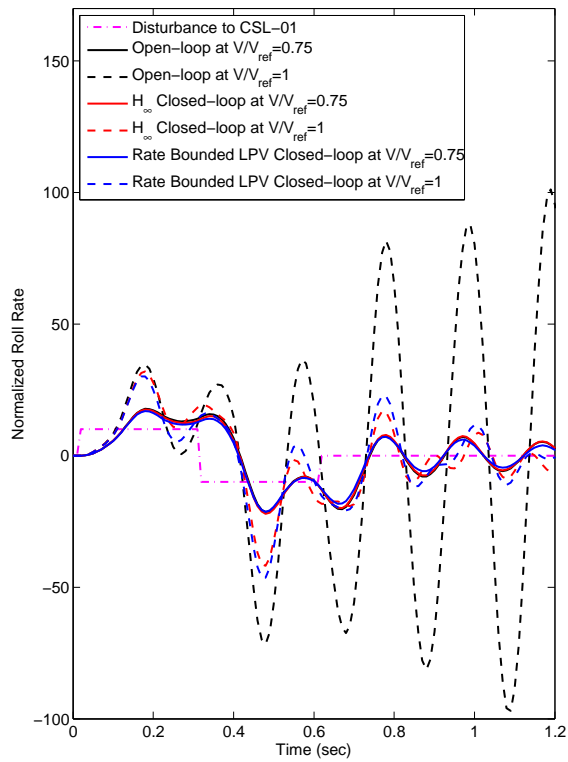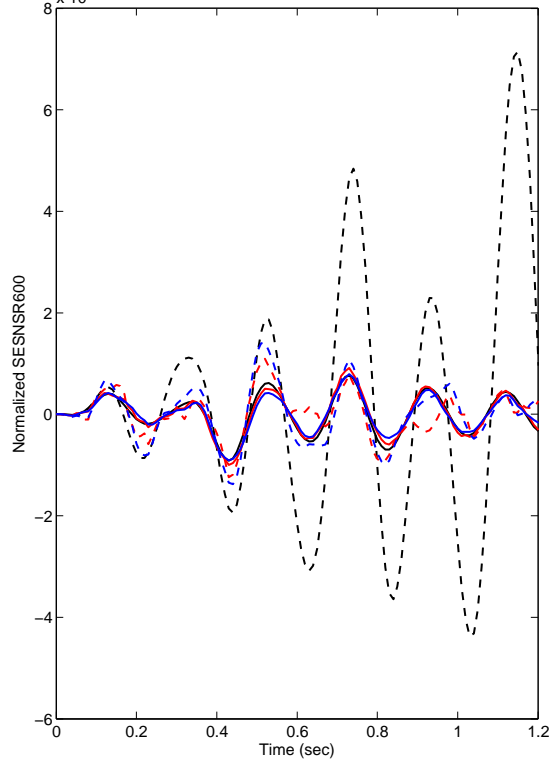
Figure 27. X-56A H_∞ and LPV Controllers with Actuators: Full Order X-56A Models, $d \rightarrow p$, $d \rightarrow$ ASENSR600
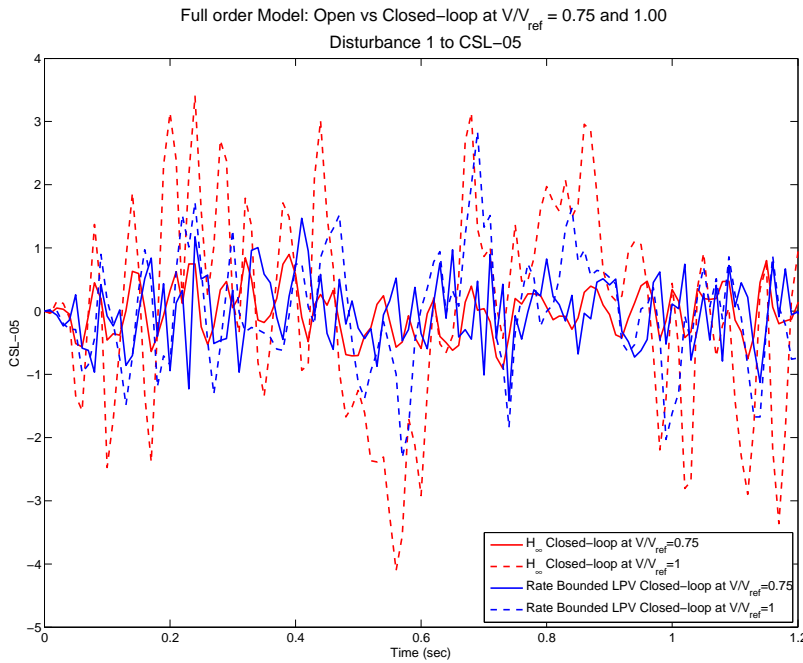
Figure 28. X-56A H_∞ and LPV Controllers with Actuators: Full Order X-56A Models, $d \rightarrow$ CSL-05

E.   X-56A Summary

The flight dynamics and control of the X-56A aircraft are considered for the vehicle flying straight and level at seven different velocities. The X-56A model considered contains 14 structural modes. The linear models of the vehicle contain 130 states which correspond to the aircraft rigid body, aeroelastic modes, unsteady aerodynamic lags and actuator states. The aircraft is stable up until $V/V_{ref} = 0.83$. The body freedom flutter mode goes unstable at $V/V_{ref} = 0.83$, the first symmetric bending becomes unstable at $V/V_{ref} = 0.92$ and the first anti-symmetric goes unstable at $V/V_{ref} = 1$. The X-56A control objective considered is stabilization of the vehicle across its flight envelope, $V/V_{ref} = 0.58$ to $V/V_{ref} = 1.08$, and augmented damping of the four aeroelastic modes between 10 and 45 rad/s.

The X-56A control design problem in this section considered the reduced order X-56A models with and without actuator models. Inclusion of the actuator models improved the performance and lowered the overall bandwidth of the control designs. H_∞ and LPV control design techniques were used to synthesize controllers across the flight envelope. Model reduction techniques were used to construct 15 state reduced order models of the X-56A with states that are consistent across the flight envelope. The H_∞ point design controllers achieved similar performance across the flight envelope, though the bandwidth of the closed-loop system varied significantly. A single, rate-bounded LPV controller was able to achieve a similar level of performance at each operating point as the H_∞ design. The LPV controller is also guaranteed to achieve this performance as the vehicle maneuvers within the flight regime. The flight control system with the LPV controller implemented has a bandwidth similar to the H_∞ designs.

VI.   Conclusion

This paper has outlined the capabilities of the LPVTOOLS software suite being developed by MUSYN Inc. A demonstration of the LPVTOOLS software was provided by an example featuring the X-56A, an aircraft with unstable aeroelastic modes. The tools were used to model the X-56A as a grid-based LPV system. Both H_∞ and grid-based LPV controllers were synthesized for the X-56A model, and their performance analyzed and compared. The LPV controller, generated by the LPVTOOLS software suite, was capable of matching the performance of H_∞ point designs across the flight envelope.

American Institute of Aeronautics and Astronautics

Acknowledgments

References

[1]Packard, A., "Gain scheduling via linear fractional transformations," *Systems and Control Letters*, Vol. 22, No. 2, 1994, pp. 79–92.

[2]Packard, A. and Kantner, M., "Gain scheduling the LPV way," *IEEE Conference on Decision and Control*, 1996, pp. 3938–3941.

[3]Scherer, C. and Weiland, S., "Linear Matrix Inequalities in Control," *DISC Lecture Notes*, 2000.

[4]Scherer, C., "LPV Control and Full Block Multipliers," *Automatica*, Vol. 37, No. 3, 2001.

[5]Apkarian, P. and Gahinet, P., "A convex characterization of gain-scheduled H_∞ controllers," *IEEE Transactions on Automatic Control*, Vol. 40, No. 5, 1995.

[6]Apkarian, P. and Gahinet, P., "Erratum to "A convex characterization of gain-scheduled H_∞ controllers"," *IEEE Transactions on Automatic Control*, Vol. 40, No. 9, 1995.

[7]Becker, G., *Quadratic Stability and Performance of Linear Parameter Dependent Systems*, Ph.D. Dissertation, University of California, Berkeley, 1993.

[8]Becker, G., Packard, A., Philbrick, D., and Balas, G., "Control of Parametrically-Dependent Linear Systems: A Single Quadratic Lyapunov Approach," *Proceedings Of The American Control Conference*, San Francisco, California, June 1993, pp. 2795–2799.

[9]Wu, F., *Control of linear parameter varying systems*, Ph.D. Dissertation, University of California at Berkeley, 1995.

[10]Wu, F., Yang, X. H., Packard, A., and Becker, G., "Induced L2-Norm Control for LPV Systems with Bounded Parameter Variation Rates," *International Journal of Robust and Nonlinear Control*, Vol. 6, 1996, pp. 2379–2383.

[11]Sun, X. and Postlethwaite, I., "Affine LPV modeling and its use in gain-scheduled helicopter control," *UKACC International Conference on Control*, 1998, pp. 1504–1509.

[12]Balas, G., Bokor, J., and Szabo, Z., "Invariant subspaces for LPV systems and their applications," *IEEE Transactions on Automatic Control*, Vol. 48, No. 11, 2003, pp. 2065–2069.

[13]Bruzelius, F. and Breitholtz, C., "Gain scheduling via affine linear parameter-varying systems and H_∞ synthesis," *IEEE Conference on Decision and Control*, 2001, pp. 713–718.

[14]Baranyi, P., Yam, Y., and Varlaki, P., *Tensor Product Model Transformation in Polytopic Model-Based Control*, Taylor & Francis, 2011.

[15]Cockburn, J. C. and Morton, B. G., "Linear Fractional Representations of Uncertain Systems," *Automatica*, Vol. 33, No. 7, 1997.

[16]Belcastro, C. and Chang, B., "LFT Formulation for Multivariate Polynomial Problems," *Proceedings of the American Control Conference*, No. June, 1998.

[17]Hecker, S., *Generation of low order LFT Representations for Robust Control Applications*, Ph.D. Dissertation, Technischen Universitat Munchen, 2006.

[18]Pfifer, H. and Hecker, S., "Generation of Optimal Linear Parametric Models for LFT-Based Robust Stability Analysis and Control Design," *IEEE Transactions on Control Systems Technology*, Vol. 19, No. 1, Jan. 2011, pp. 118–131.

[19]Pfifer, H., *LPV/LFT Modeling and its Application in Aerospace*, Ph.d. dissertation, Technischen Universität München, 2013.

[20]Mohammadpour, J. and Scherer, C. W., editors, *Control of Linear Parameter Varying Systems with Applications*, Springer US, Boston, MA, 2012.

[21]Lee, L. H., *Identification and Robust Control of Linear Parameter-Varying Systems*, Ph.D. Dissertation, University of California at Berkeley, 1997.

[22]Glover, K., "All Optimal Hankel Norm Approximations of Linear Multivariable Systems and their L_∞ Error Bounds," *International Journal of Control*, Vol. 39, 1984, pp. 1115–1193.

[23]Ravi, R., Pascoal, A., and Khargonekar, P., "Normalized Coprime Factorization for Linear Time Varying Systems," *Systems and Control Letters*, Vol. 18, 1992, pp. 455–465.

[24]Wood, G. D., *Control of Parameter-Dependent Mechanical Systems*, Ph.d. dissertation, University of Cambridge, 1995.

[25]Wood, G. D., Goddard, P. J., and Glover, K., "Approximation of Linear Parameter-Varying Systems," *IEEE Conference on Decision and Control*, 1996.